Microglial NKCC1 shapes microglial phenotype, cerebral inflammatory responses and brain injury

Krisztina Tóth[1,2], Nikolett Lénárt[1], Eszter Szabadits[1], Balázs Pósfai[1,2], Rebeka Fekete[1], Csaba Cserép[1], Ahmad Alatshan[3,4], Szilvia Benkő[3, 4], Christian A. Hübner[5], Kai Kaila[6], Zsuzsanna Környei[1] and Ádám Dénes[1,]*

[1] Momentum Laboratory of Neuroimmunology, Institute of Experimental Medicine, Budapest, H-1083 Hungary

[2] János Szentágothai Doctoral School of Neuroscience, Semmelweis University, Budapest, H-1083 Hungary

[3] Department of Physiology, Faculty of Medicine, University of Debrecen, Debrecen, H-4012 Hungary

[4] Doctoral School of Molecular Cellular and Immune Biology, Faculty of Medicine, University of Debrecen, Debrecen, H-4012 Hungary

[5] University Hospital Jena of Friedrich Schiller University, Jena, 07737 Germany

[6] Molecular and Integrative Biosciences and Neuroscience Center (HiLIFE), University of Helsinki, Helsinki, 00014 Finland

[*] Correspondence: denes.adam@koki.hu

Abstract

The NKCC1 ion transporter contributes to the pathophysiology of common neurological disorders, but its function in microglia, the main inflammatory cells of the brain, has not been studied to date. Therefore, we generated a novel transgenic mouse line in which microglial NKCC1 was deleted. We show that microglial NKCC1 shapes both baseline and reactive microglia morphology and inflammatory responses. As opposed to systemic NKCC1 blockade, which decreased intracortical lipopolysaccharide (LPS)-induced cytokine levels, neuroinflammation was potentiated by both intracortically administered bumetanide and in the absence of microglial NKCC1, suggesting a considerable role for microglia to influence central NKCC1 actions. Correspondingly, microglial NKCC1 KO animals exposed to experimental stroke showed significantly increased brain injury, inflammation, cerebral edema and worse neurological outcome. Thus, NKCC1 emerges as an important player to shape microglial responses and brain inflammation after CNS injury, which is likely to be relevant for common neurological disorders.

Introduction

Ion regulation in the brain's extracellular milieu is maintained by transporters and ion channels with a key contribution of Na^+/K^+-ATPase. NKCC1 (Na^+-K^+-Cl^- co-transporter 1) mediates the secondary active transport of Na^+, K^+ and 2 Cl^- ions into the cells, which is driven by sodium and potassium gradients. This electroneutral transport is balanced by the function of the Cl^- extruder KCC2. Both transporters contribute to broad and heterogenous biological processes, including cell volume regulation, neuronal development, maturation and synapse formation, while they are also essential to sustain low intracellular Cl^- levels in mature neurons (Ben-Ari, 2002; Kaila et al., 2014; Rivera et al., 1999; Yamada et al., 2004). NKCC1 is implicated in a number of neuropathological conditions, including neonatal seizures, temporal lobe epilepsy, autism spectrum disorders, schizophrenia, and brain edema after traumatic or hypoxic/ischaemic injury (Garneau et al., 2020; Huang et al., 2019b; Kahle et al., 2008; Kaila et al., 2014). However, the cellular targets for central NKCC1 actions remain to be characterized.

Experimental and clinical studies using the loop diuretic bumetanide to antagonize NKCC1 in various neurological and psychiatric conditions reported positive therapeutic effects or variable outcomes (Ben-Ari et al., 2016; Damier et al., 2016; Hadjikhani et al., 2018; Kaila et al., 2014; Kharod et al., 2019; Lemonnier et al., 2012; Marguet et al., 2015; Pressler et al., 2015; Puskarjov et al., 2014). Notably, the poor pharmacokinetic properties of bumetanide, including a low permeability across the blood brain barrier (BBB), have raised numerous questions about its cellular targets in the CNS (Römermann et al., 2017; Töllner et al., 2015). Among these, actions of bumetanide on NKCC1 expressed by non-neural cells have been suggested to explain some of its central effects (Garneau et al., 2020; Kharod et al., 2019; Puskarjov et al., 2014). In fact, NKCC1 expression in the CNS has been confirmed in several non-neuronal cell types (Virtanen et al., 2020), such as choroid plexus epithelial cells, ependymal cells (Gregoriades et al., 2019; Steffensen et al., 2018), astrocytes (Henneberger et al., 2020; Hui et al., 2016; Noor et al., 2019; Su et al., 2002) and oligodendrocytes (Wang et al., 2003; Yu et al., 2018). Interestingly, common neurological disorders involving altered NKCC1 activity (Liu et al., 2020) also

display broad neuroinflammatory changes. While the impact of NKCC1 function on inflammatory cytokine production has not been widely studied, emerging evidence indicates upregulated NKCC1 expression in response to inflammatory stimuli (LPS, IL-1β, TNF-α) (Huang et al., 2019b, 2014; Pozdeev et al., 2017; Reid et al., 2013; Weidenfeld and Kuebler, 2017). However, while microglia are the main inflammatory cell type in the CNS, there is no information about the functional role of NKCC1 in microglia and whether microglial NKCC1 could provide a significant contribution to central NKCC1 actions under inflammatory conditions or after brain injury.

Altered microglial activity is linked with the pathophysiology of most common brain disorders, such as neurodegenerative and psychiatric diseases, stroke and epilepsy (Salter and Stevens, 2017; Song and Colonna, 2018). While the extracellular accumulation of potassium is related to diverse neuropathological alterations, the contribution of microglial potassium channels and transporters to microglial activity is widely recognized. These include membrane-expressed potassium channels (Kv1.3, THIK-1, Kir2.1) that regulate microglial motility, immune surveillance and cytokine release, among others (Kharod et al., 2019; Madry et al., 2018; Nguyen et al., 2017). Moreover, changes in intracellular potassium levels are associated with inflammasome activation contributing to the regulation of IL-1β release (Di et al., 2018; He et al., 2016). Interestingly, recent transcriptomic data verified high-level NKCC1 expression in microglia (DePaula-Silva et al., 2019; Swertz et al., 2010; Zhang et al., 2014). However, currently no experimental data are available to demonstrate the function of microglial NKCC1 under physiological and pathological conditions. To this end, we studied whether central and systemic NKCC1 blockade impact on central inflammatory changes differently and tested the hypothesis that NKCC1 is involved in the regulation of microglial inflammatory mediator production, neuroinflammation and brain injury.

Results

Systemic and intracortical blockade of NKCC1 oppositely regulate LPS-induced inflammatory cytokine production in the brain

To investigate whether systemic blockade of NKCC1 actions by bumetanide could alter inflammatory responses in the CNS, we injected mice either intraperitoneally (ip.) or intracortically with bacterial lipopolysaccharide (LPS), while NKCC1 actions were blocked by systemic (intraperitoneal; ip.) bumetanide administration (Figure 1A). As expected, LPS administration by ip. injection triggered marked inflammation in the spleen (Supplementary Figure 1A), but low cytokine production in cortical brain tissues, which was not influenced by ip. bumetanide treatment (Figure 1A). However, bumetanide resulted in a small, but significant increase in LPS-induced IL-1β production in the spleen (Supplementary Figure 1A). Importantly, while intracortical LPS administration triggered a robust inflammatory response in the brain as seen earlier (Giles et al., 2018, 2015), ip. bumetanide treatment reduced intracortical LPS-induced inflammation. This was demonstrated by lower GCSF, KC, IL-1β, and IL-1α levels in the brain (by 39.8%, 43%, 54.6% and 41%, respectively), while systemic cytokine levels were not altered (Supplementary Figure 1A).

Next, we investigated the impact of intracortical bumetanide administration on LPS-induced cytokine responses, by co-injecting bumetanide with LPS (Figure 1B) into the cerebral cortex. As expected, intracortical LPS resulted in a 20-50-fold increase in inflammatory cytokines/chemokines in the cerebral cortex compared to vehicle (saline). Surprisingly, bumetanide markedly increased LPS-induced GCSF, KC, IL-1β and IL-1α levels in the brain (by 86.1%, 31.2%, 82.5% and 72.4%, respectively) as opposed to the effects of ip. bumetanide treatment (Figure 1A). Intracortical bumetanide had no effect on systemic cytokine levels (Supplementary Figure 1B).

We next tested whether the effects of intracortical bumetanide administration on cytokine production might be explained by altered LPS-induced recruitment of leukocytes. Flow cytometry revealed

increased number of infiltrating $CD45^{high}$ leukocytes, in particular $CD11b^{+}$ $Ly6G^{high}$ granulocytes, and $CD11b^{+}$ $Ly6G^{-}$ $Ly6C^{high}$ monocytes in response to intracortical LPS injection compared to vehicle administration (Figure 1C-D), which was not altered by intracortical bumetanide administration. The number of $CD45^{int}$ $CD11b^{+}$ microglia was not affected either (Figure 1C-D), indicating that the increased LPS-induced cytokine production observed upon intracortical bumetanide treatment is not due to altered inflammatory cell numbers in the cerebral cortex.

Microglia are the primary source of inflammatory cytokines in a number of neuropathologies, and IL-1β, also produced by microglia, is a key proinflammatory cytokine regulating the brain's cytokine network (Allan et al., 2005; Heneka et al., 2014). To investigate the cellular source of IL-1β in this experimental model, we injected LPS intracortically into $Cx3CR1^{+/GFP}$ (microglia reporter) mice. Multi-label immunostainings confirmed that Cx3CR1-GFP microglia coexpressing P2Y12R and CD45 displayed IL-1α and IL-1β in their cytoplasm (Figure 1E). Thus, these findings collectively suggested that microglia are likely to be major mediators of central bumetanide actions under inflammatory conditions.

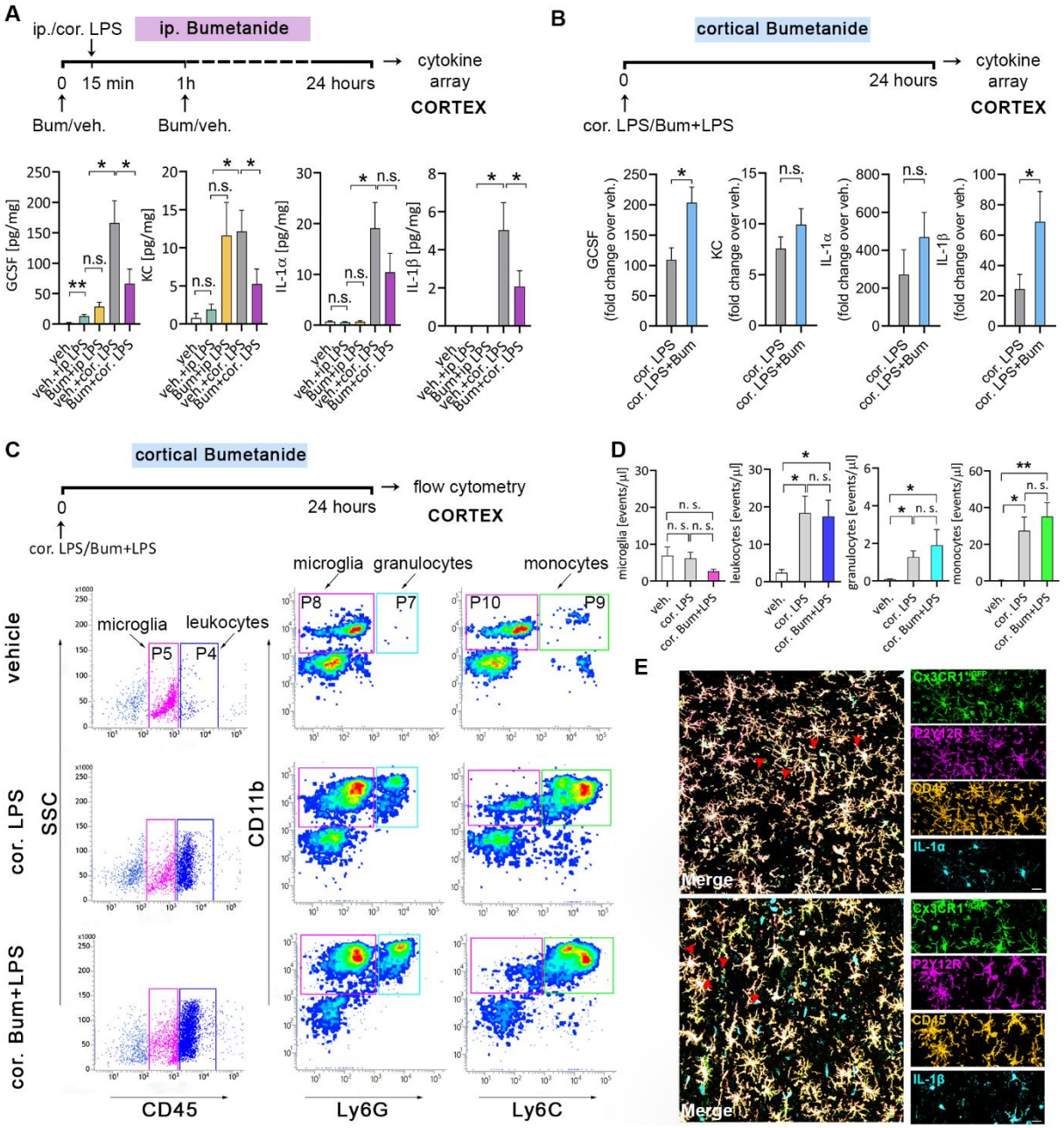

Figure 1. Systemic and intracortical blockade of NKCC1 oppositely regulates LPS-induced inflammatory cytokine production in the brain. A: Mice were subjected to either intraperitoneal (ip.) or intracortical (cor.) LPS injections, while NKCC1 was blocked by ip. bumetanide (Bum) administration. Central LPS injection triggers high cytokine responses in the brain compared to ip. LPS injection, which is blocked by ip. Bum administration. **B:** Central NKCC1 inhibition by intracortical Bum administration significantly increases GCSF and IL-1β levels. See also Supplementary Figure 1 for effects of systemic vs. central blockade of NKCC1 on LPS-induced cytokine responses in the periphery. **C-D:** Flow cytometric dot plots show that cortical administration of Bum does not affect the number of microglia ($CD45^{int}$/P5 gate), and recruitment of leukocytes ($CD45^{high}$/P4 gate), monocytes ($CD11b^{+}$, $Ly6C^{high}$ /P9 gate), or granulocytes ($CD11b^{+}$, $Ly6G^{high}$/P7 gate) upon central LPS injection. **E:** The main source of IL-1α and IL-1β in the brain are microglia cells. Confocal images of $Cx3CR1^{+/GFP}$ brain slices show IL-1α-CD45-P2Y12R (above, red arrowheads) and IL-1β-CD45-P2Y12R (below, red arrowheads) labeled cells after cortical LPS injection-induced inflammation. All data are expressed as mean±SEM. **A:** One-way ANOVA followed by Tukey's multiple comparison test; *p<0.05; N=6/group; **B:** Unpaired t-test;

*p<0.05; N=9/group; **D:** One-way ANOVA followed by Tukey's multiple comparison test; *p<0.05; N=4/group. **E:** Scale: 25 µm Abbreviations: veh.: vehicle; ip: intraperitoneal; cor.: cortical; Bum: bumetanide; n. s.: not significant

Microglia-specific deletion of NKCC1 markedly impacts on baseline cell morphology and alters transformation to reactive microglia

Available RNA-seq data demonstrate that the *Slc12a2* gene is expressed by microglia (DePaula-Silva et al., 2019; Swertz et al., 2010; Zhang et al., 2014). In line with this, our qPCR data revealed that mRNA levels of NKCC1 in microglial cells isolated from newborn (1.052±0.054) or adult (0.89±0.098) C57BL/6J mice are comparable to that in neural progenitors derived from embryonic brains (1.30±0.05; Figure 2A). However, NKCC1 mRNA expression dramatically decreased when cells were grown in culture for 10 days (Figure 2A), making it difficult to study NKCC1 function in microglia using *in vitro* techniques. To study the functional role of NKCC1 in microglia *in vivo*, we generated a novel transgenic mouse line in which microglial NKCC1 was deleted (Figure 2B). *Slc12a2* expression in isolated microglia derived from tamoxifen-inducible microglia-specific NKCC1 KO mice was markedly reduced in comparison with wild type littermates (WT: 1.46±0.11, KO: 0.50±0.016; Figure 2C) as assessed by qPCR. Reduced NKCC1 protein expression was also confirmed by immunofluorescent stainings, which revealed a discrete NKCC1-labeling in the plasma membrane of microglial cells in WT mice, which was absent in microglia-specific NKCC1 KO mice (Figure 2D-E).

Microglia are known to respond to physiological and pathological challenges with fast morphological transformation, while the role of NKCC1 in cell volume regulation has been highlighted in previous studies concerning other cell types (Heindl et al., 2018; Kahle et al., 2015). To study the role of NKCC1 in microglial cell shape, we performed automated morphological analysis using perfusion-fixed brain sections obtained from WT and microglia-specific NKCC1 KO mice (Figure 2F-I). First, we aimed to test whether microglial NKCC1 deficiency has any impact on baseline cell morphology. Our data revealed that NKCC1-deficient microglia acquired 23.8% higher cell surface, 19% higher branch volume, and 33.5% more branches compared to WT cells (Figure 2F and 2H), while we observed no changes in the

cell body volume of KO versus WT microglia (Figure 2H). Next, we examined the morphological characteristics after inflammatory activation that leads to altered microglial responses and morphological transformation (Wendeln et al., 2018). Both WT and NKCC1 KO microglia responded to intracortical LPS administration with dramatic morphological conversion (Figure 2G and 2I). However, activated NKCC1-deficient microglia were significantly smaller than their wild type counterparts, displaying a 10% smaller cell surface, 12.5% smaller cell volume and 13.7% smaller branch volume (Figure 2I). According to these data, microglial NKCC1 is likely to be involved both in shaping baseline cell morphology and regulation of cell volume after inflammatory challenges.

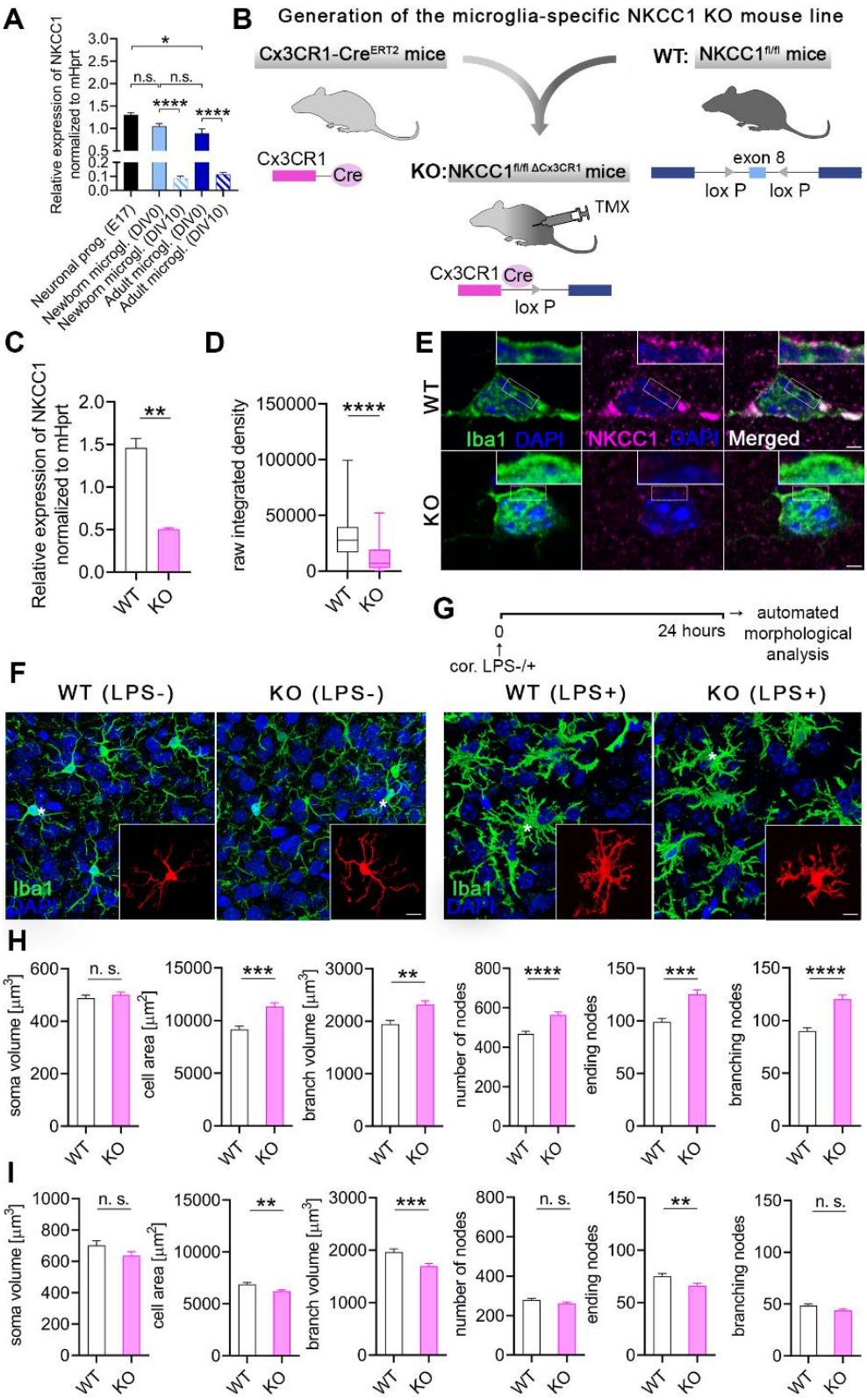

Figure 2. Microglia-specific deletion of NKCC1 markedly impacts on baseline cell morphology and alters transformation to reactive microglia. A: NKCC1 mRNA expression levels in newborn and adult microglia isolated from C57BL/6J mice compared to neural progenitors derived from E17 embryonic hippocampi. Note, that NKCC1 mRNA levels decrease dramatically during *in vitro* maintenance (DIV10). **B:** We generated a novel microglia-specific conditional NKCC1 KO transgenic mouse line by crossing NKCC1$^{fl/fl}$ (exon 8 of the *Slc12a2* gene was flanked with lox P sites) and Cx3CR1-Cre^{ERT2} mice. **C:** NKCC1

mRNA levels in isolated NKCC1 KO microglia was markedly reduced in comparison to wild type cells. **D-E:** NKCC1 protein expression in NKCC1 KO microglia cells is markedly reduced compared to WT cells. Inserts show plasma membrane localization of NKCC1. **F-G:** Experimental outline of automated morphological analysis and maximum intensity projections of confocal images. Inserts show cells marked with white asterisks in 3D. **H:** Automated morphological analysis shows that features of NKCC1 deficient microglia significantly differ from WT microglia **I:** Activated NKCC1 deficient microglia are slightly smaller than their wild type counterparts. All parametric data are expressed as mean±SEM. **A:** One-way ANOVA, followed by Holm-Sidak's post hoc test. N=3/group. **: $p<0.01$; n.s.: not significant **C:** Mann-Whitney test, N=3/group. **: $p<0.01$ **D:** Mann-Whitney test, N (WT)=142 cells from 2 mice, N (KO)=83 cells from 1 mouse. ****: $p<0.0001$ **E:** Scale: 2 µm **F-G:** Scale:10 µm **H:** Mann-Whitney test, N (WT)=78 cells from 3 mice, N (KO)=136 cells from 5 mice. **: $p<0.01$, ***: $p<0.001$, ****: $p<0.0001$ **I:** Mann-Whitney test, N (WT)=171 cells from 6 mice, N (KO)=85 cells from 4 mice. **: $p<0.01$, ***: $p<0.001$ Abbreviations: DIV: days in vitro; n.s.: not significant; TMX: tamoxifen; cor.: cortical

The absence of microglial NKCC1 boosts inflammatory cytokine production in the cerebral cortex in response to an inflammatory stimulus

To test the impact of NKCC1 on the regulation of microglial activity, we examined LPS-induced cytokine production in NKCC1 KO and WT mice. Twenty-four hours after intracortical LPS injections, we measured several cytokines and chemokines from brain homogenates (Figure 3A). Importantly, deletion of microglial NKCC1 markedly potentiated LPS-induced levels of GCSF (3.53-fold), KC (2.12-fold), IL-1α (3.98-fold), IL-1β (3.96-fold), IL-6 (4.35-fold) and TNF-α (3-fold) in the cerebral cortex compared to WT (Figure 3A). In contrast, intracortical LPS treatment did not alter cytokine levels or in T cell, B cell, monocyte or granulocyte numbers in the spleen (Supplementary Figure 2A-C). Similarly to that seen after intracortical pharmacological inhibition of NKCC1 by bumetanide, neither the number of $CD11b^{+}$ $CD45^{int}$ microglial cells nor blood-borne $CD11b^{+}$ $CD45^{high}$ leukocytes, $CD11b^{+}$ $Ly6C^{high}$ monocytes or $CD11b^{+}$ $Ly6G^{high}$ granulocytes were altered as a result of microglial NKCC1 deficiency (Figure 3B-C). These findings corroborated our previous results on cortical bumetanide blockade, confirming that microglial NKCC1 is an important mediator of central cytokine production upon inflammatory challenges.

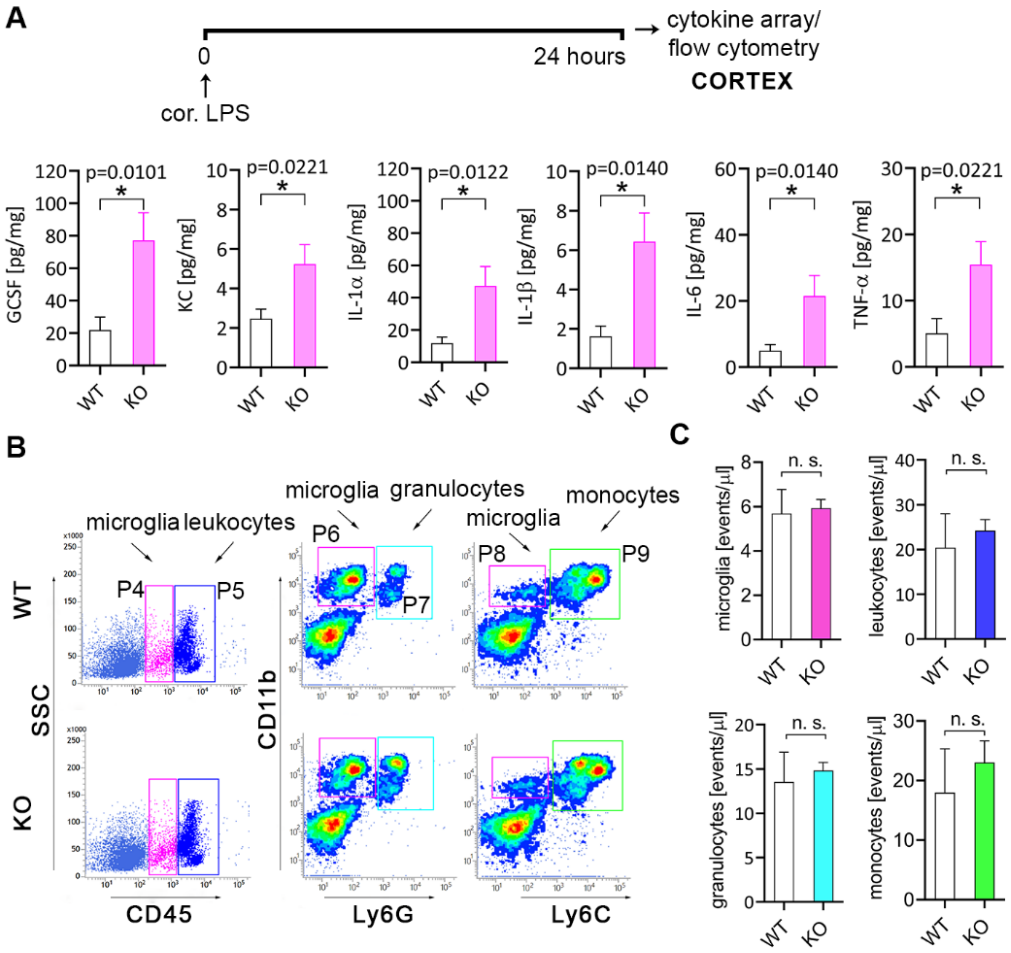

Figure 3. The absence of microglial NKCC1 boosts inflammatory cytokine production in the cerebral cortex in response to an inflammatory stimulus. A: LPS-induced cytokine levels are significantly higher in the cortices of microglia-specific NKCC1 KO mice than in WT. **B-C:** Flow cytometric dot plots show that microglial NKCC1 deficiency does not alter the number of $CD11b^{+}$, $CD45^{int}$ microglia (P4 gate) or numbers of infiltrating $CD11b^{+}$, $CD45^{high}$ leukocytes (P5 gate), $CD11b^{+}$, $Ly6C^{high}$ monocytes (P9 gate) and $CD11b^{+}$, $Ly6G^{high}$ granulocytes (P7 gate) in response to intracortical LPS administration**.** See corresponding data on peripheral cytokine levels and immune cell populations in Supplementary Figure 2**. A:** Mann-Whitney test, *: p <0.05; N (WT)=7, N (KO)=6; **C:** unpaired t-test, N (WT)=4, N (KO)=4; n. s.: not significant.

Deletion of microglial NKCC1 increases infarct volume, brain edema and worsens neurological outcome after MCAo

Because Na^{+}-coupled Cl^{-} importers and their upstream regulatory serine-threonine kinases (WNK-SPAK-OSR1) are involved in maintaining intracellular ionic homeostasis as well as regulation of cell volume homeostasis (Alessi et al., 2014; Russell, 2000), inhibiting these co-transporters is a subject of interest in ischemic stroke therapy and in other forms of acute brain injury (brain trauma, SAH) where

cerebral edema is a major contributor to poor clinical outcome (Kahle et al., 2008). Thus, we investigated whether microglial NKCC1 deficiency influences the severity of brain injury after experimental stroke in microglia-specific NKCC1 KO mice subjected to transient, 45 min long middle cerebral artery occlusion (MCAo). Twenty-four hours after reperfusion, we observed a significant increase in brain edema, which was accompanied by a 47% increase in lesion volume (Figure 4A-B; p=0.0262) and poor neurological outcome in NKCC1 KO mice (Figure 4B; Bederson's score: WT: 1.17±0.17, KO: 2.0±0.24; Composit neurological score: WT: 14.9±1.65, KO: 21.9±2.12). Furthermore, experimental stroke induced a 4-fold upregulation of IL-1α and 4.8-fold increase in IL-1β expressing NKCC1 KO microglia cells compared to WT animals, while the overall microglia density and the number of activated microglia were not different at 24h reperfusion (Figure 4D-E). We also assessed whether increases in IL-1 production take place early after brain injury before the majority of the infarct is formed. Cytometric bead array did not reveal altered cytokine production in cortical homogenates shortly (8 hours) after MCAo (Figure 4C). Taken together, these results indicate that microglial NKCC1 deficiency results in augmented brain inflammation, brain edema and increased brain injury after experimental stroke.

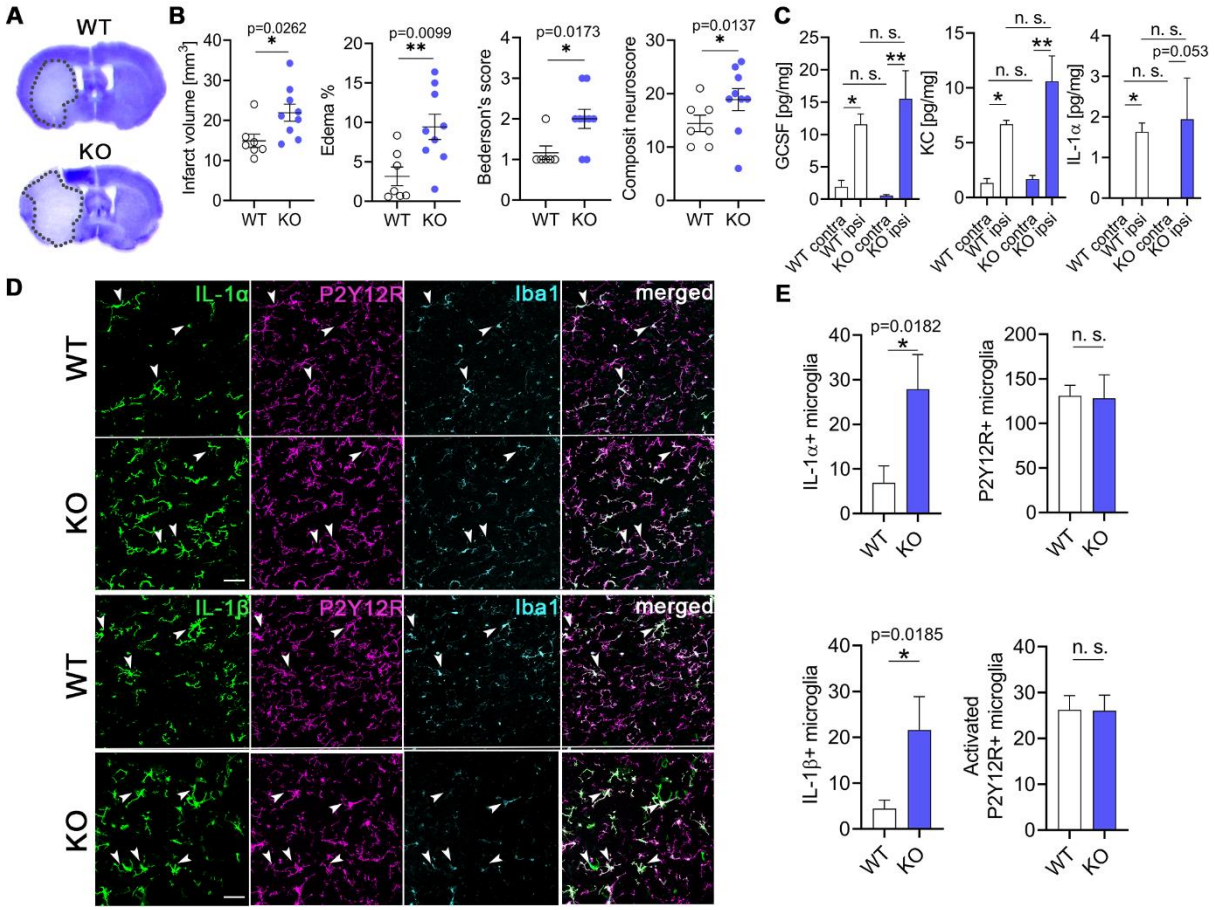

Figure 4. Deletion of microglial NKCC1 increases infarct volume, brain edema and worsens neurological outcome after MCAo. A-B: Microglial NKCC1-deficient mice (KO) show larger infarct volume as assessed on cresyl violet-stained brain sections and more severe neurological outcome compared to wild type mice. **C:** Cytokine levels in the cortex do not differ 8 hours after MCAo in KO mice compared to WT. **D-E:** Microglial NKCC1 deletion results in higher levels of IL-1α and IL-1β 24 hours after MCAo. **B:** Unpaired t-test, N (WT)=7, N (KO)=9; *: $p<0.05$, **: $p<0.01$ **C:** Kruskall-Wallis test followed by Dunn's multiple comparison test; N=6/group. *: $p<0.05$, **: $p<0.01$ **D:** Scale: 50 µm **E:** Mann-Whitney test, *: $p<0.05$; N (WT)=7, N (KO)=9. n.s.: not significant

Discussion

To our knowledge, we show for the first time that NKCC1 is functionally active in microglia in the adult mouse brain and that microglial NKCC1 is involved in shaping both baseline and reactive microglia morphology and responses. While systemic NKCC1 blockade attenuates LPS-induced inflammation in the brain, central pharmacological or microglia-specific NKCC1 blockade potentiates inflammatory cytokine production. Microglia-specific NKCC1 deletion also increases brain injury, inflammation,

cerebral edema, and leads to worse neurological outcome after acute brain injury induced by experimental stroke. Thus, microglial NKCC1 emerges as an important regulator of neuroinflammation, suggesting that NKCC1 may be involved in regulating microglia activation and central inflammatory responses to a wide range of pathological stimuli.

Previous studies have reported that disturbances in chloride transporter functions during development or in the adult brain can severely affect neuronal functioning. An increase in NKCC1 expression leads to disrupted Cl^- homeostasis, resulting in depolarizing GABA actions in various neurological/psychiatric conditions (Kahle et al., 2008). Altered NKCC1 function has been implicated in epilepsy or neuronal hyperexcitability and its involvement in the pathophysiology of cerebral ischemia, neuropathic pain, fragile X syndrome, post-stroke depression, schizophrenia or autism spectrum disorders has also been suggested (Ben-Ari, 2017; Huang et al., 2019a; Puskarjov et al., 2014; Schulte et al., 2018; Wu et al., 2020; Zhang et al., 2020). Several attempts have been made to treat chloride dysregulation by antagonizing neuronal NKCC1 in order to lower internal Cl^- levels and promote GABA-induced hyperpolarization (Ben-Ari, 2017; Kaila and Miles, 2010; Schulte et al., 2018). For that purpose, the loop diuretic bumetanide, a selective antagonist of NKCC1, has predominantly been used (Kharod et al., 2019; Puskarjov et al., 2014). Bumetanide was reported to reduce seizure frequency after traumatic brain injury and epilepsy, or to attenuate symptoms of autism spectrum disorders and brain edema (Ben-Ari, 2017; Ben-Ari et al., 2016; Hadjikhani et al., 2018; Kharod et al., 2019; Puskarjov et al., 2014), while it has led to conflicting results in other studies. For instance, bumetanide was reported inefficacious in neonatal hypoxic-ischemic encephalopathy (Pressler et al., 2015) and in schizophrenic patients (Rahmanzadeh et al., 2017). Possible explanations for the varying efficiency of bumetanide treatment in either in clinical trials or in experimental models include the high affinity of bumetanide to serum albumin, its short half-life in the serum and the brain, and poor penetration across the BBB (Puskarjov et al., 2014; Römermann et al., 2017; Töllner et al., 2015). Therefore, effects of systemic bumetanide treatment on different cellular targets are likely to be dependent on the actual doses of

the drug in different compartments of the CNS, which could be influenced by the level of BBB permeability associated with a given neurological condition (Auer et al., 2020; Huang et al., 2019a).

To unravel NKCC1-mediated actions in the periphery and the brain, we investigated the systemic vs. central effects of bumetanide in response to bacterial endotoxin (LPS) administration, which is widely used to trigger inflammatory cytokine responses (Giles et al., 2018; Wendeln et al., 2018). Intraperitoneally injected bumetanide reduced intracortical LPS-induced proinflammatory cytokine/chemokine responses in the brain, similarly to that found in the case of LPS-induced lung injury attributed to NKCC1-mediated macrophage activation (Hung et al., 2020). These findings are also consistent with the beneficial therapeutic effects of systemic NKCC1 blockade in CNS pathologies, as reported in several studies, which could be partially due to anti-inflammatory actions.

However, the precise cellular targets of systemic NKCC1 blockade concerning its therapeutic effects in different CNS pathologies, are not well understood. In addition to neuronal NKCC1 actions, effects on diverse cell types throughout the periphery (see review by Garneau et al.), hormonal or peripheral nerve-mediated central actions (Garneau et al., 2020; Watanabe and Fukuda, 2015), or the involvement of cellular elements of the neurovascular unit (e.g. endothelial cells or perivascular macrophages) and glial cells (Virtanen et al., 2020) should also be considered. Importantly, intracortical administration of bumetanide had just the opposite effect on intracortical LPS-induced cytokine production to that seen after systemic bumatenide treatment, resulting in elevated cytokine levels in the cortex. Because microglia are key contributors to inflammatory cytokine production in the brain, we tested whether microglial activity could be directly related to NKCC1 function. Indeed, we observed comparable *Slc12a2* expression in microglia, isolated from either newborn or adult mouse brains, to that seen in neural progenitors. We also revealed NKCC1 protein in cortical microglial cells, which is in line with recent observations showing microglial NKCC1 expression in the superficial spinal dorsal horn in rats (Javdani et al., 2020). Microglial NKCC1 expression is also supported by a large number of single-cell transcriptomic studies set together in the BRAIN-SAT database (Swertz et al., 2010). Interestingly,

Slc12a2 is not expressed by bone marrow-derived macrophages recruited into the brain (DePaula-Silva et al., 2019).

To investigate the cell-autonomous effects of NKCC1 in microglia, we generated a new, microglial NKCC1 KO transgenic mouse line. After intracortical LPS administration, cytokine production was markedly augmented in the absence of microglial NKCC1, verifying our previous results on cortical NKCC1 inhibition by bumetanide. Potassium efflux across the plasma membrane is required for the production of IL-1β upon NLRP3 inflammasome activation (Di et al., 2018; He et al., 2016; Swanson et al., 2019). The TWIK2 two-pore domain K^+ channel (K_{2P}) has recently been identified as the actual K^+ efflux channel triggering NLRP3 activation in lung macrophages (Di et al., 2018). While RNA profiling (Butovsky et al., 2014; Zhang et al., 2014) revealed high expression of TWIK2 in microglia, based on physiological characteristics, another K_{2P} channel, namely THIK-1, has been identified as the main K^+ channel in microglia (Madry et al., 2018). Blocking THIK-1 function was shown to inhibit the release of IL-1β from activated microglia, consistent with potassium efflux being necessary for inflammasome activation. Thus, it is possible that enhanced cytokine production observed in microglial NKCC1 deficient animals may be partially due to changes in K^+ efflux mechanisms, but other processes, including altered cell volume regulation, Toll-like receptor- and inflammasome signaling, or microglial process dynamics could also be responsible for this effect.

Proinflammatory cytokine production, particularly the effects mediated by IL-1, are known to influence acute brain injury induced by brain trauma or stroke (Brough and Denes, 2015; Lambertsen et al., 2012; Luheshi et al., 2011; Wofford et al., 2019). We found significantly increased infarct volume (by 47%) in microglia-specific NKCC1 KO mice after experimental stroke comparable to a striking, 60% increase in infarct size caused by highly efficient, selective microglia elimination (Szalay et al., 2016). Microglia depletion resulted in dysregulated neuronal network activity, an effect that is likely to be mediated via elimination of protective microglia-neuron interactions at somatic purinergic junctions (Cserép et al., 2020). We suggest that in line with BBB injury and impaired ion balance upon ischemia, disruption of

NKCC1 transporter function is likely to result in microglial dysfunction in the early phases of cerebral ischemia, which may be complemented with increased IL-1 production that collectively influences brain injury. This may be supported by the findings that we could not detect increased cytokine production in the absence of microglial NKCC1 early (8h) after MCAo, while both IL-1α and IL-1β expression were markedly upregulated in NKCC1 KO microglia 24 hours after reperfusion. While the actual contribution of IL-1 to brain injury was not investigated in the present study, earlier findings have shown blunted ischemia-induced proinflammatory cytokine production in microglia deficient animals (Szalay et al., 2016), suggesting a considerable role of impaired protective microglial responses in brain injury in microglial NKCC1 KO animals. Our results also suggest that the widely observed protective effects of systemic NKCC1 blockade in different CNS pathologies may be counterbalanced by microglial NKCC1 actions, therefore the net effect of NKCC1 blockade could be markedly influenced by the effective concentrations of NKCC1 inhibitors in the brain parenchyma. This highlights the importance of future studies using conditional mouse models to investigate the precise sites of NKCC1 actions in the brain, to better explain contradictions in the present literature.

Following stroke, impaired cell volume regulation results in cytotoxic cell swelling and edema formation. Cerebral edema was shown to be associated with increased phosphorylation of the SPAK/OSR1 kinases playing a key role in NKCC1 activation in various neural cell types (Begum et al., 2015; Kahle et al., 2015; O'Donnell et al., 2004) and a SPAK kinase inhibitor, ZT-1a, attenuated cerebral edema after stroke (Zhang et al., 2020). In line with this, NKCC1 is involved in homeostatic cell volume regulation (Alessi et al., 2014; Demian et al., 2019; Russell, 2000; Shekarabi et al., 2017) and bumetanide attenuates edema formation in response to ischaemic or traumatic brain injury (Huang et al., 2019b; Hui et al., 2016; O'Donnell et al., 2004). While we could not detect major differences in soma volumes between resting or LPS-activated WT and NKCC1 KO cells *in vivo*, microglia-specific deletion of NKCC1 considerably impacted on cell morphology. Unfortunately, our trials to assess NKCC1-mediated microglial volume regulation *in vitro* have failed due to the significant downregulation of NKCC1 expression under cell culture conditions, a phenomenon reported previously

(Bohlen et al., 2017; Butovsky et al., 2014). The significance of our *in vivo* data on cell morphology is supported by the findings that NKCC1 ion co-transporter function is associated with actin cytoskeleton dynamics (Ma et al., 2019; Schiapparelli et al., 2017) by controlling F-actin organization through Cofilin-1 and RhoGTPase activity (Schiapparelli et al., 2017). Interestingly, it has recently been shown that LTP-triggered withdrawal of perisynaptic astroglial processes depends on NKCC1 and cofilin actions (Henneberger et al., 2020). It remains to be investigated with *in vivo* imaging, whether microglial process motility or translocation of the cell body in the brain is influenced by NKCC1 activity.

In conclusion, we show that microglial NKCC1 plays a previously unrecognized role in shaping microglial phenotype and inflammatory responses. Strikingly, bumetanide-induced enhancement of neuroinflammation was mimicked by conditional deletion of microglial NKCC1, suggesting that microglial NKCC1 is a significant target of bumetanide in those cases where high enough concentrations of the drug are reached within brain tissue. Our results also suggest that microglial NKCC1 activity may be required to control neuroinflammation and edema formation in the injured brain. Therefore, the contribution of microglial NKCC1 and other cellular sites of NKCC1 actions should be considered when studying the therapeutic effects of NKCC1 inhibitors in different CNS pathologies. Given the broad clinical interest in pharmacological NKCC1 blockade, as well as the widespread clinical application of the loop diuretic bumetanide, we suggest that microglial NKCC1-mediated effects should be extensively investigated in both experimental and clinical studies. The present results call for a re-evaluation of the pharmacological effects of bumetanide in brain diseases with a significant neuroinflammatory component.

Materials and Methods

Experimental animals

Experiments were performed on adult male C57BL/6J (RRID: IMSR JAX:000664), NKCC1$^{fl/fl}$ and NKCC1$^{fl/fl\ \Delta\ Cx3CR1}$ (microglia-specific NKCC1 knockout), mice (all on C57BL/6J background). For experiments using LPS treatment P90-110, and for MCAo experiments P70-90 day old mice were used. NKCC1$^{fl/fl}$ mice were kindly provided by Dr. Christian A. Hübner of University Hospital Jena of Friedrich Schiller University, Jena, Germany. Ubiquitous NKCC1 KO mice (P15-20, NKCC1 full knockout, NKCC1$^{-/-}$), generated by crossing C57BL/6NTac-Gt(ROSA)26Sor$^{tm16(cre)Arte}$ and NKCC1$^{fl/fl}$ mice, were used as immunostaining controls and were not subjected to other experimental procedures. Mice were housed in a 12 hours dark/light cycle environment, under controlled temperature and humidity and *ad libitum* access to food and water. All experimental procedures were in accordance with the guidelines set by the European Communities Council Directive (86/609 EEC) and the Hungarian Act of Animal Care and Experimentation (1998; XXVIII, Sect. 243/1998), approved by the Animal Care and Experimentation Committee of the Institute of Experimental Medicine and the Government Office of Pest Country Department of Food Chain Safety, Veterinary Office, Plant Protection and Soil Conservation Budapest, Hungary under the number PE/EA/1021- 7/2019 and Department of Food Chain Safety and Animal Health Directorate of Csongrád Country, Hungary. All experiments followed ARRIVE and IMPROVE guidelines (Kilkenny et al., 2010; Percie du Sert et al., 2017). A code was allocated to each animal using GraphPad's random number generator and was randomly assigned to different treatment groups. During all surgical procedures and functional tests the experimenter was blinded to the treatment.

Generation and genotyping of the microglia-specific NKCC1 knockout mouse line

Microglia-specific NKCC1 deletion (NKCC1$^{fl/fl\ \Delta Cx3CR1}$) was achieved by crossing tamoxifen-inducible B6.129P2(C)-CX3CR1tm2.1 (cre/ERT2)Jung/J mice (RRID:IMSR_JAX:020940JAX) (Yona et al., 2013) with the NKCC1$^{fl/fl}$ mouse line (Antoine et al., 2013), in which a region between exon 7 and exon 10 of

Slc12a2 gene was flanked with lox P sites. Microglia-specific NKCC1 deletion was achieved by two intraperitoneally administered tamoxifen injections (2 mg/100 µl in corn oil, #T5648, Sigma-Aldrich) 48 hours apart in 3-4 weeks old male mice, shortly after weaning. In all experiments, conditional mutant mice heterozygous for cre and homozygous for NKCC1 flox ($^{cre/+\ fl/fl}$), referred to as NKCC1 KO throughout the manuscript, were used. In all cases, littermate controls - referred to as WT - were used which were negative for cre and homozygous for NKCC1 flox ($^{+/+\ fl/fl}$). Heterozygous, conditional mutant mice were viable, fertile, average in size, and did not display any gross physical or marked behavioral abnormalities. Genotypes for *Slc12a2* encoding NKCC1 were determined from tail biopsy samples by conventional PCR using the following primers: 5'-GCAATTAAGTTTGGAGGTTCCTT, 5'-CCAACAGTATGCAGACTCTC and 5'-CCAACAGTATGCAGACTCTC; product sizes: 200 bps for WT, 260 bps for floxed and 460 bps for KO.

Microglia cell preparations and cultures

Microglia cells from either newborn (P0-1, male or female) or adult (P40-55, male) C57BL/6J, NKCC1$^{fl/fl}$ (WT) or NKCC1$^{fl/fl\ \Delta\ Cx3CR1}$ (KO) mice were isolated by magnetic separation using anti-CD11b microbeads (Miltenyi Biotec, Germany), with slight modification of the protocol described by Otxoa-de-Amezaga (Otxoa-de-Amezaga et al., 2019). After transcardial perfusion with ice-cold PBS (phosphate buffered saline), the brain tissues (cortices and hippocampi) were enzymatically dissociated with Neural Tissue Dissociation Kit-P (#130-092-628; Miltenyi Biotec). Myelin was removed by MACS Myelin Removal Beads II (#130-096-733, Miltenyi Biotec), then cells in a single-cell suspension were magnetically labeled with MACS CD11b microbeads (#130-093-634, Miltenyi Biotec) and were separated using MS columns (#130-042-201, Miltenyi Biotec, Germany). Cells selected with CD11b microbeads were plated onto poly-L-lysine precoated 96-well or 386-well plates at $3x10^4$ cell/cm^2 density and were cultured at 37 °C in a 95% air/5% CO_2 incubator in DMEM/Glutamax medium (#31966-021, Gibco) supplemented with 10% FBS (fetal bovine serum, #FB-1090, Biosera), 1% Pen/Strep (10000 U/ml; #15140-122,

ThermoFisher Scientific) and 10 nM Macrophage Colony-Stimulating Factor (M-CSF; #PMC2044, ThermoFisher Scientific) for 10 days.

Embryonic neural progenitor cell preparations

Embryonic hippocampal cells were prepared from C57BL/6J mice on embryonic day 17. After aseptically removing the hippocampi from the skull, tissue was freed from meninges and incubated in 0.05% trypsin-EDTA (#T4549, Sigma-Aldrich) solution with 0.05% Dnase I (#DN25, Sigma-Aldrich) in phosphate-buffered saline (PBS) for 15 min at 37°C.

Intracortical injections

P90-110 mice were deeply anesthetized with fentanyl (0.05 mg/kg) and mounted into a stereotaxic frame, then were subjected to either single saline or LPS (lipopolysaccharide from *Escherichia coli* O26:B6; 200 nl of 5 mg/ml, rate=200 nl/10 min; #L8274, Sigma-Aldrich) injections using a glass micropipette (Giles et al., 2018). The coordinates for the injection were anterior-posterior -2,5 mm, lateral +1,5 mm, and ventral -0,25 mm from the bregma. Bumetanide, a specific inhibitor of NKCC1 was co-injected with LPS (50 µM; #3108, Tocris). At 24h, mice were transcardially perfused with saline, and approximately 0.5x0.5x0.5 cm sized tissue pieces from the center of each injected cortical region were cut off and collected for cytokine array and flow cytometric analysis. For tissue sectioning mice were perfused with saline followed by 4% paraformaldehyde in PBS.

Systemic administration of LPS and bumetanide

Male adult NKCC1$^{fl/fl}$ mice were injected intraperitoneally with saline, LPS (2 mg/kg; O26:B6, #L8274, Sigma-Aldrich) or LPS (2 mg/kg) and bumetanide (25 mg/kg; #3108, Tocris). Intraperitoneal bumetanide injections were repeated twice, the first one 15 min prior to LPS injection, the second one 1 hour after LPS administration. The double injection aimed to ensure that in the critical time window we have effective concentrations of bumetanide in the circulation. At 24h, saline-perfused spleen and brain samples were collected for cytokine measurements or flow cytometric analysis.

Cytokine measurement

The levels of inflammatory cytokines and chemokines were measured in spleen and brain samples. Sample processing and protein determination were performed as described previously (Denes et al., 2015). Mice were transcardially perfused with saline prior to the collection of spleen and brain samples (ipsilateral to injections). Tissue samples were homogenized in TritonX-100 and protease inhibitor-containing (1:100, #539131, Calbiochem) Tris-HCl buffer (TBS, pH 7.4) and centrifuged at 17000 g, for 20 min at 4 °C. Protein level was quantified for every sample using BCA Protein Assay Kit (#23225, ThermoFisher Scientific). Then, measured cytokine levels were normalized for total protein concentrations. The concentrations of cytokines and chemokines were determined by BD™ Cytometric Bead Array (CBA) using BD CBA Flex Sets (GCSF: #560152, KC: #558340, IL-1α: #560157, IL-1β: #560232, IL-6: #558301, TNF-α: #558299, BD, Becton, Dickinson and Company) according to the manufacturer's instructions. Samples were acquired using a BD FACSVerse flow cytometer (BD, Becton, Dickinson and Company) and the results were analyzed by FCAP Array software (BD, Becton, Dickinson and Company).

Flow cytometric analysis of brain and spleen samples

For flow cytometric analysis, cells were isolated from mouse brains with Collagenase D (0,5 mg/ml, #11088866001, Roche), DNase I (10µg/ml, #DN25, Sigma-Aldrich) dissolved in 10% FBS containing DMEM (#6546, Sigma-Aldrich), then the cell suspension was passed through a 40 µm cell strainer (Corning). After enzymatic dissociation, the cells were resuspended in 40% Percoll solution and overlayed on 70% Percoll (#17-0891-01, GE Healthcare). After a density centrifugation step (at 2100 rpm, 30 min), mononuclear cells were collected from the interphase of 40%/70% Percoll. Spleen was mechanically homogenized and red blood cells were removed by centrifugation. Before acquisition, brain and spleen cells were diluted with FACS buffer and were incubated with anti-mouse CD16/32 to block Fc receptor. Brain cells or spleen leukocytes were incubated with cocktails of selected antibodies: T cells - anti-mouse CD8a-PE (1:200, #12-0081-82, eBioscience), anti-mouse CD3-APC clone 17A2

(1:200, #17-0032-80, eBioScience), anti-mouse CD4-FITC (1:200, #11-0043-82, eBioscience), anti-mouse CD45-PerCP/Cy5.5 (1:200, #103131, BioLegend); B cells/granulocytes - anti-mouse CD19-FITC (1:200, #11-0193-81, eBioScience), anti-mouse Ly-6C-PE-Cy7 (1:500, #25-5932-80, eBioScience), anti-mouse Ly-6G-APC (1:500, #127613, BioLegend); monocytes/granulocytes - anti-mouse CD11b-FITC (1:200, #11-0112-81, eBioscience); anti-mouse Ly-6C-PE-Cy7; anti-mouse Ly-6G-APC, CD45-PerCP/Cy5.5. To exclude dead cells, some coctails contained propidium iodide (3 µM; #P1304MP, ThermoFisher). Cells were acquired on a BD FACSVerse flow cytometer and data were analyzed using FACSuite software (BD, Becton, Dickinson and Company). Cell counts were calculated by using 15 µm polystyrene microbeads (#18328-5, Polysciences).

RNA isolation and cDNA reverse transcription

For qRT-PCR measurements, CD11b+ magnetic sorted microglia cells or embryonic neural progenitor cells were homogenized in QIAzol Lysis Reagent (#79306, QIAGEN) either immediately after isolation or after 10 days of in vitro culturing. Total RNA was isolated using Direct-zol™ RNA Miniprep Kits (#R2052, Zymo Research) following the manufacturer's protocol. The RNA purity and concentration were assessed by NanoDrop ND-1000 spectrophotometer (Nanodrop Technologies). The isolated RNA was then stored at −80 °C. RNA was subjected to DNase I (#AM2224, Ambion) treatment in the presence of RNase H inhibitor (#AM2682, Ambion). Standardized quantities of RNA were reverse transcribed to cDNA using the SuperScript™ II First-strand Reverse Transcriptase system (#18064014, ThermoFisher Scientific) and random hexamers (#48190011, Invitrogen) supplemented with RNase H inhibitor (#AM2682, Ambion).

Real-time quantitative PCR (qRT-PCR)

Real-time quantitative PCR was performed with QuantStudio12K Flex qPCR instrument (Applied Biosystems), using TaqMan Gene Expression Assays and the TaqMan Gene Expression Master Mix (#4369016, ThermoFischer Scientific). All mouse TaqMan Gene Expression Assays used for amplification reactions were obtained from ThermoFischer Scientific: *Slc12a2* (Mm01265951_m1,

targeting exon 1-10); (Mm00436546_m1, targeting exon 8-10, used for the validation of microglia specific NKCC1 deletion, see Figure 2C), *Hprt* (Mm03024075_m1). The amplification was performed under the following cycling conditions: 95 °C for 10 min, followed by 40 cycles of 95 °C for 10 sec, and 60 °C for 1 min. The comparative Ct method (ΔΔCt method) was used to analyze the relative expression values for each transcript using Hprt as a reference gene.

Middle cerebral artery occlusion (MCAo)

To assess the functional contribution of microglial NKCC1 to ischemic brain injury, mice were subjected to a 45 min long MCAo (Middle Cerebral Artery occlusion) using a silicone-coated filament, as described earlier by Dénes et al. (Dénes et al., 2010). Surgery was performed under isoflurane (1,5% in a 30% O_2 and 70% N_2O gas mixture) anesthesia and core body temperature was tightly controlled (37 °C ± 0.5 °C) during the whole procedure using a homeothermic heating blanket. Laser Doppler flowmetry was used to validate the occlusion of the MCA. In brief, after a midline incision made on the ventral surface of the neck, the right common carotid artery (CCA) was isolated and a silicone-coated monofilament (210-230 µm tip diameter, Doccol, Sharon, US) was introduced to the left external carotid artery (ECA) and advanced along the internal carotid artery (ICA) to occlude the MCA. Animals were kept in a post-operative chamber at 26-28 °C until the functional assessment having free access to mashed food and water. Neurological outcome was assessed at 24h reperfusion using corner test and the 5-point Bederson's sensory- motor deficit scoring system (Bederson et al., 1986; Iadecola et al., 1997; Schaar et al., 2010). Briefly, the following scores were given: a 0, no motor deficit; 1, flexion of torso and contralateral forelimb when mouse was lifted by the tail; 2, circling to the contralateral side when mouse is held by the tail on a flat surface, but normal posture at rest; 3, leaning to the contralateral side at rest, 4, no spontaneous motor activity, 5, early death due to stroke. Functional outcome has also been assessed by a complex neurological scoring system to obtain a more comprehensive readout (Orsini et al., 2012). Results are expressed as composite neurological score. Composite scores range from 0 (healthy mice) to 56 (worst performance) by adding up scores from 13

categories as follows: hair (0–2), ears (0–2), eyes (0–4), posture (0–4), spontaneous activity (0–4), and epileptic behavior (0–12), and focal deficits: body symmetry (0–4), gait (0–4), climbing on a surface held at 45° (0–4), circling behavior (0–4), front limb symmetry (0–4), compulsory circling (0–4), and whisker response to a light touch (0–4).

Infarct volume and brain edema were calculated after 24h survival on cresyl violet stained coronal brain sections using ImageJ as described previously (McColl et al., 2007). In brief, lesion volume was determined at eight neuro-anatomically defined coronal levels (between +2 mm rostral and -4 mm caudal to bregma) by integrating measured areas of damage and correcting for edema-size. The pre-determined inclusion criteria for analysis were as follows; decline in Doppler signal of at least 70%, no cerebral hemorrhages and survival to 24 h. Cerebral hemorrhage was identified post-mortem by the presence of excessive bleeding on the external surface of the brain, typically close to the filament location.

Immunohistochemistry

Perfusion, tissue processing and immunostaining for histology

Mice were anesthetized and transcardially perfused with 0.9% NaCl solution for 1 minute, followed by 4% PFA in 0.1 M phosphate buffer (PB) for 40 minutes, followed by 0.1 M PB for 10 minutes to wash the fixative out. Blocks containing the primary somatosensory cortex and dorsal hippocampi were dissected, and coronal sections were prepared on a vibratome (VT1200S, Leica, Germany) at 50 µm thickness for immunofluorescent histological and 100 µm thickness for the automated morphological analysis. Sections were washed in 0.1 M PB, incubated in 10%- and 30%-sucrose containing 0.1 M PB for 3 and 12 hours, respectively. Then the samples were placed into cryovials, snap frozen in liquid nitrogen, and stored at -80 °C for further use. For the free-floating immunohistochemical detection of NKCC1 each vial contained sections from NKCC1$^{fl/fl}$ (WT), NKCC1$^{fl/fl\ \Delta Cx3CR1}$ (KO) and NKCC1$^{-/-}$ mice, which sections were marked by different cuts, enabling that all experimental parameters were completely identical for all samples. The sections were washed in TBS, blocked with a Mouse-on-Mouse blocker

solution (MOM blocker, #BMK-2202, Vectorlabs) for 1 hour, washed in TBS 2x5 minutes, washed with MOM-diluent 2x5 minutes. The diluted anti-NKCC1 primary antibodies (NKCC1 Rb: 1:4000, #13884-1-AP, Proteintech, NKCC1 M: 1:2000, diluted in MOM-diluent; DSHB) were pre-incubated for 48 hours with brain slices from NKCC1$^{-/-}$ mice, in order to remove the fraction of immunoglobulins that could potentially cause aspecific-binding. After discarding these slices, the guinea pig anti-Iba1 antibody (#234004, Synaptic Systems) was added to reach a 1:1000 final dilution. This antibody-mixture was applied on the samples for 48 hours at 4 °C during gentle shaking. After intensive washes in TBS, sections were incubated with a mixture of secondary antibodies (donkey-anti mouse Alexa 647, 1:1000, #715-605-150; donkey-anti rabbit Alexa 488, 1:1000, #711-546-152; donkey-anti guinea pig Alexa 594, 1:1000, #706-586-148; Jackson ImmunoResearch, diluted in TBS) for 24 hours. After subsequent washes in TBS and 0.1 M PB, DAPI staining was performed and the sections were mounted on glass slides, and covered with Diamond Antifade (#P36961, ThermoFisher) or Aquamount (#18606-5, Polysciences). Immunofluorescence was analyzed using a Nikon Eclipse Ti-E inverted microscope (Nikon Instruments Europe B.V., Amsterdam, The Netherlands), with a CFI Plan Apochromat VC 60X oil immersion objective (numerical aperture: 1.4) and an A1R laser confocal system. We used 405, 488, 561 and 647 nm lasers (CVI Melles Griot), and scanning was done in line serial mode. Single image planes were exported from the ND2 files, the outline of microglial cells was drawn using the Iba1-labeling, and the integrated density of the NKCC1 fluorescence signal was measured within these respective ROI-s. This section is related to Figure 2.

Perfusion, processing and immunostaining of ischaemic tissues

In terminal ketamine-xylazine anesthesia (100 mg/kg-10 mg/kg) mice were transcardially perfused with 0.9% NaCl solution, followed by 4% phosphate buffered PFA. Brains of microglia-specific NKCC1 KO mice subjected to 45 min MCAo were postfixed and cryoprotected overnight (in 4% phosphate buffered PFA-10% sucrose solution), then immersed into a cryoprotective solution (10% sucrose in PBS) at least 2h before 25 µm coronal sections were cut using a sledge microtome. Immunofluorescent

staining was performed on free-floating coronal brain sections. Brain sections were blocked with 5% normal donkey serum followed by overnight incubation at 4 °C using the following mixture of primary antibodies: goat anti-IL-1β/ILF2 (1:250; #AF-401-NA, R&D Systems), rat anti-CD45 (1:250; #MCA1388, AbD Serotec), rabbit anti-P2Y12R (1:500; #55043AS, AnaSpec). After the incubation with the primaries, sections were washed several times in TBS and were incubated with mixture of corresponding secondary antibodies at room temperature for 2h. The following secondaries were used: donkey-anti goat CF568 (1:1000; #20106, Biotium), donkey-anti rabbit Alexa 647 (1:1000; #711-605-152, Jackson ImmunoResearch), donkey-anti rat Alexa 488 (1:1000; #712-546-153, Jackson ImmunoResearch). Slices were washed in TBS and were mounted to microscope slides using Fluoromount-G (#0100-01, SouthernBiotech). Representative images were captured with a 20X objective (Plan Apo VC, numerical aperture: 0,.75, FOV=645.12um) on a Nikon A1R confocal system. Quantitative analysis was performed on widefield images, captured with a 20X objective (Plan, numerical aperture: 0.4) on a Nikon Eclipse Ti-E inverted microscope (Nikon Instruments Europe B.V., Amsterdam, The Netherlands). IL-1α and IL-1β positive cells in the penumbral region, P2Y12R positive and CD45 positive cells in the whole cortex were counted on 3-3 serial coronal sections for a given brain area. This methodical description is related to Figure 4.

Automated morphological analysis of microglial cells

100 µm thick mouse brain coronal sections were immunostained with guinea pig anti-Iba1 (1:500; #234004, Synaptic Systems), Alexa 647 donkey anti-guinea pig (1:500; #706-606-148, Jackson ImmunoResearch) antibodies, and DAPI. Imaging was carried out in 0.1M PB, using a Nikon Eclipse Ti-E inverted microscope (Nikon Instruments Europe B.V., Amsterdam, The Netherlands), with a CFI Plan Apochromat VC 60X water immersion objective (numerical aperture: 1.2) and an A1R laser confocal system. For 3-dimensional morphological analysis of microglial cells, the open-source MATLAB-based Microglia Morphology Quantification Tool was used (available at https://github.com/isdneuroimaging/mmqt). This method uses microglia and cell nuclei labeling to

identify microglial cells. Briefly, 59 possible parameters describing microglial morphology are determined through the following automated steps: identification of microglia (nucleus, soma, branches) and background, creation of 3D skeletons, watershed segmentation and segregation of individual cells (Heindl et al., 2018).

Quantification and Statistical analysis

All quantitative assessment was performed in a blinded manner. Based on the type and distribution of data populations (examined with Shapiro-Wilk normality tests) we applied appropriate statistical tests: In the case of two independent groups, Student's t-test or Mann-Whitney U-test, for three or more independent groups one-way ANOVA followed by Tukey's *post hoc* comparison or Kruskal-Wallis test with Dunn's multiple comparison test was applied. Data were analyzed using the GraphPad Prism version 8.2 for Windows software (GraphPad Software, San Diego, California USA). In this study, data are expressed as mean±SEM, $p<0.05$ was considered statistically significant.

Acknowledgments

This work was supported by „Momentum" research grant from the Hungarian Academy of Sciences (LP2016-4/2016 to A.D.) and ERC-CoG 724994 (to A.D.). Additionally, this work was funded by Hungarian National Scientific Research Fund (NKFIH-OTKA Grant No. K131844 to S.B.), the János Bolyai Research Scholarship of the Hungarian Academy of Sciences (to N.L. and C.C.), ÚNKP-20-3-II (to B.P.) and ÚNKP-20-5 (to C.C.) of the New National Excellence Program of the Ministry for Innovation and Technology, Hungary; and German Research Foundation (SPP 1665) and the Federal Ministry of Education and Research (NEURON ACRoBAT) to C.A.H. A.A. holds a Stipendium Hungaricum Scholarship from the Government of Hungary. We thank László Barna and the Nikon Imaging Center at the Institute of Experimental Medicine for kindly providing microscopy support, and thank Dóra Gali-Györkei for her excellent technical assistance.

Author Contributions

Experimental design and overall concept, A.D. and Zs.K; Methodology, C.A.H.; N.L.; E.S.; Formal Analysis K.T.; N.L., B.P., S.B.; Investigation, K.T., N.L., B.P., R.F., E.S., A.A., C.C, Z.K.; Resources, A.D., S.B., C.A.H; Writing – Original Draft, K.T., Z.K., A.D., Writing – Review & Editing K.T.; Z.K., A.D. with all authors; Intellectual contribution, conceptual support K.K., C.A.H; Visualization K.T., E.S., C.C., B.P.; Supervision A.D. and Zs.K.; Project Administration A.D. and Zs.K.; Funding Acquisition, A.D.

Competing interests

The authors declare no competing interests.

References

Alessi DR, Zhang J, Khanna A, Hochdörfer T, Shang Y, Kahle KT. 2014. The WNK-SPAK/OSR1 pathway: Master regulator of cation-chloride co-transporters. *Sci Signal*. doi:10.1126/scisignal.2005365

Allan SM, Tyrrell PJ, Rothwell NJ. 2005. Interleukin-1 and neuronal injury. *Nat Rev Immunol*. doi:10.1038/nri1664

Antoine MW, Hübner CA, Arezzo JC, Hébert JM. 2013. A causative link between inner ear defects and long-term striatal dysfunction. *Science (80-)* **341**:1120–1123. doi:10.1126/science.1240405

Auer T, Schreppel P, Erker T, Schwarzer C. 2020. Impaired chloride homeostasis in epilepsy: Molecular basis, impact on treatment, and current treatment approaches. *Pharmacol Ther*. doi:10.1016/j.pharmthera.2019.107422

Bederson JB, Pitts LH, Tsuji M, Nishimura MC, Davis RL, Bartkowski H. 1986. Rat middle cerebral artery occlusion: Evaluation of the model and development of a neurologic examination. *Stroke* **17**:472–476. doi:10.1161/01.STR.17.3.472

Begum G, Yuan H, Kahle KT, Li L, Wang S, Shi Y, Shmukler BE, Yang S Sen, Lin SH, Alper SL, Sun D. 2015. Inhibition of WNK3 Kinase Signaling Reduces Brain Damage and Accelerates Neurological Recovery after Stroke. *Stroke* **46**:1956–1965. doi:10.1161/STROKEAHA.115.008939

Ben-Ari Y. 2017. NKCC1 Chloride Importer Antagonists Attenuate Many Neurological and Psychiatric Disorders. *Trends Neurosci*. doi:10.1016/j.tins.2017.07.001

Ben-Ari Y. 2002. Excitatory actions of gaba during development: the nature of the nurture. *Nat Rev Neurosci* **3**:728–739. doi:10.1038/nrn920

Ben-Ari Y, Damier P, Lemonnier E. 2016. Failure of the nemo trial: Bumetanide is a promising agent to treat many brain disorders but not newborn seizures. *Front Cell Neurosci* **10**. doi:10.3389/fncel.2016.00090

Bohlen CJ, Bennett FC, Tucker AF, Collins HY, Mulinyawe SB, Barres BA. 2017. Diverse Requirements for Microglial Survival, Specification, and Function Revealed by Defined-Medium Cultures. *Neuron* **94**:759-773.e8. doi:10.1016/j.neuron.2017.04.043

Brough D, Denes A. 2015. Interleukin-1α and brain inflammation. *IUBMB Life*. doi:10.1002/iub.1377

Butovsky O, Jedrychowski MP, Moore CS, Cialic R, Lanser AJ, Gabriely G, Koeglsperger T, Dake B, Wu PM, Doykan CE, Fanek Z, Liu L, Chen Z, Rothstein JD, Ransohoff RM, Gygi SP, Antel JP, Weiner HL. 2014. Identification of a unique TGF-β-dependent molecular and functional signature in microglia. *Nat Neurosci* **17**:131–143. doi:10.1038/nn.3599

Cserép C, Pósfai B, Lénárt N, Fekete R, László ZI, Lele Z, Orsolits B, Molnár G, Heindl S, Schwarcz AD, Ujvári K, Környei Z, Tóth K, Szabadits E, Sperlágh B, Baranyi M, Csiba L, Hortobágyi T, Maglóczky Z, Martinecz B, Szabó G, Erdélyi F, Szipocs R, Tamkun MM, Gesierich B, Duering M, Katona I, Liesz A, Tamás G, Dénes Á. 2020. Microglia monitor and protect neuronal function through specialized somatic purinergic junctions. *Science (80-)* **367**:528–537. doi:10.1126/science.aax6752

Damier P, Hammond C, Ben-Ari Y. 2016. Bumetanide to Treat Parkinson Disease. *Clin Neuropharmacol* **39**:57–59. doi:10.1097/WNF.0000000000000114

Demian WL, Persaud A, Jiang C, Coyaud É, Liu S, Kapus A, Kafri R, Raught B, Rotin D. 2019. The Ion Transporter NKCC1 Links Cell Volume to Cell Mass Regulation by Suppressing mTORC1. *Cell Rep* **27**:1886-1896.e6. doi:10.1016/j.celrep.2019.04.034

Denes A, Coutts G, Lénárt N, Cruickshank SM, Pelegrin P, Skinner J, Rothwell N, Allan SM, Brough D. 2015. AIM2 and NLRC4 inflammasomes contribute with ASC to acute brain injury independently of NLRP3. *Proc Natl Acad Sci U S A* **112**:4050–4055. doi:10.1073/pnas.1419090112

Dénes Á, Humphreys N, Lane TE, Grencis R, Rothwell N. 2010. Chronic systemic infection exacerbates ischemic brain damage via a CCL5 (regulated on activation, normal T-cell expressed and secreted)-mediated proinflammatory response in mice. *J Neurosci* **30**:10086–10095. doi:10.1523/JNEUROSCI.1227-10.2010

DePaula-Silva AB, Gorbea C, Doty DJ, Libbey JE, Sanchez JMS, Hanak TJ, Cazalla D, Fujinami RS. 2019. Differential transcriptional profiles identify microglial- and macrophage-specific gene markers expressed during virus-induced neuroinflammation. *J Neuroinflammation* **16**:152. doi:10.1186/s12974-019-1545-x

Di A, Xiong S, Ye Z, Malireddi RKS, Kometani S, Zhong M, Mittal M, Hong Z, Kanneganti TD, Rehman J, Malik AB. 2018. The TWIK2 Potassium Efflux Channel in Macrophages Mediates NLRP3 Inflammasome-Induced Inflammation. *Immunity* **49**:56-65.e4. doi:10.1016/j.immuni.2018.04.032

Garneau AP, Slimani S, Fiola MJ, Tremblay LE, Isenring P. 2020. Multiple Facets and Roles of Na + -K + -Cl − Cotransport: Mechanisms and Therapeutic Implications. *Physiology*

35:415–429. doi:10.1152/physiol.00012.2020

Giles JA, Greenhalgh AD, Davies CL, Denes A, Shaw T, Coutts G, Rothwell NJ, Mccoll BW, Allan SM. 2015. Requirement for interleukin-1 to drive brain inflammation reveals tissue-specific mechanisms of innate immunity. *Eur J Immunol* **45**:525–530. doi:10.1002/eji.201444748

Giles JA, Greenhalgh AD, Denes A, Nieswandt B, Coutts G, McColl BW, Allan SM. 2018. Neutrophil infiltration to the brain is platelet-dependent, and is reversed by blockade of platelet GPIbα. *Immunology* **154**:322–328. doi:10.1111/imm.12892

Gregoriades JMC, Madaris A, Alvarez FJ, Alvarez-Leefmans FJ. 2019. Genetic and pharmacological inactivation of apical Na+-K+-2Cl- co-transporter 1 in choroid plexus epithelial cells reveals the physiological function of the co-transporter. *Am J Physiol - Cell Physiol* **316**:C525–C544. doi:10.1152/ajpcell.00026.2018

Hadjikhani N, Åsberg Johnels J, Lassalle A, Zürcher NR, Hippolyte L, Gillberg C, Lemonnier E, Ben-Ari Y. 2018. Bumetanide for autism: More eye contact, less amygdala activation. *Sci Rep* **8**:1–8. doi:10.1038/s41598-018-21958-x

He Y, Zeng MY, Yang D, Motro B, Núñez G. 2016. NEK7 is an essential mediator of NLRP3 activation downstream of potassium efflux. *Nature* **530**:354–357. doi:10.1038/nature16959

Heindl S, Gesierich B, Benakis C, Llovera G, Duering M, Liesz A. 2018. Automated morphological analysis of microglia after stroke. *Front Cell Neurosci* **12**. doi:10.3389/fncel.2018.00106

Heneka MT, Kummer MP, Latz E. 2014. Innate immune activation in neurodegenerative disease. *Nat Rev Immunol*. doi:10.1038/nri3705

Henneberger C, Bard L, Panatier A, Reynolds JP, Kopach O, Medvedev NI, Minge D, Herde MK, Anders S, Kraev I, Heller JP, Rama S, Zheng K, Jensen TP, Sanchez-Romero I, Jackson CJ, Janovjak H, Ottersen OP, Nagelhus EA, Oliet SHR, Stewart MG, Nägerl UV, Rusakov DA. 2020. LTP Induction Boosts Glutamate Spillover by Driving Withdrawal of Perisynaptic Astroglia. *Neuron*. doi:10.1016/j.neuron.2020.08.030

Huang H, Bhuiyan MIH, Jiang T, Song S, Shankar S, Taheri T, Li E, Schreppel P, Hintersteininger M, Yang S Sen, Lin SH, Molyneaux BJ, Zhang Z, Erker T, Sun D. 2019a. A Novel Na+-K+-Cl- Co-transporter 1 Inhibitor STS66∗ Reduces Brain Damage in Mice After Ischemic Stroke. *Stroke* **50**:1021–1025. doi:10.1161/STROKEAHA.118.024287

Huang H, Song S, Banerjee S, Jiang T, Zhang J, Kahle KT, Sun D, Zhang Z. 2019b. The WNK-SPAK/OSR1 Kinases and the Cation-Chloride Cotransporters as Therapeutic Targets for Neurological Diseases. *Aging Dis* **10**:626. doi:10.14336/ad.2018.0928

Huang LQ, Zhu GF, Deng YY, Jiang WQ, Fang M, Chen CB, Cao W, Wen MY, Han YL, Zeng HK. 2014. Hypertonic saline alleviates cerebral edema by inhibiting microglia-derived TNF-α and IL-1β-induced Na-K-Cl Co-transporter up-regulation. *J Neuroinflammation* **11**. doi:10.1186/1742-2094-11-102

Hui H, Rao W, Zhang L, Xie Z, Peng C, Su N, Wang K, Wang L, Luo P, Hao Y, Zhang S, Fei Z. 2016. Inhibition of Na+-K+-2Cl- Cotransporter-1 attenuates traumatic brain injury-induced

neuronal apoptosis via regulation of Erk signaling. *Neurochem Int* **94**:23–31. doi:10.1016/j.neuint.2016.02.002

Hung CM, Peng CK, Yang S Sen, Shui HA, Huang KL. 2020. WNK4–SPAK modulates lipopolysaccharide-induced macrophage activation. *Biochem Pharmacol* **171**. doi:10.1016/j.bcp.2019.113738

Iadecola C, Zhang F, Casey R, Nagayama M, Elizabeth Ross M. 1997. Delayed reduction of ischemic brain injury and neurological deficits in mice lacking the inducible nitric oxide synthase gene. *J Neurosci* **17**:9157–9164. doi:10.1523/jneurosci.17-23-09157.1997

Javdani F, Hegedűs K, Miranda CO, Hegyi Z, Holló K, Antal M. 2020. Differential expression of Na+/K+/Cl− co-transporter 1 in neurons and glial cells within the superficial spinal dorsal horn of rodents. *Sci Rep* **10**. doi:10.1038/s41598-020-68638-3

Kahle KT, Khanna AR, Alper SL, Adragna NC, Lauf PK, Sun D, Delpire E. 2015. K-Cl co-transporters, cell volume homeostasis, and neurological disease. *Trends Mol Med*. doi:10.1016/j.molmed.2015.05.008

Kahle KT, Staley KJ, Nahed B V., Gamba G, Hebert SC, Lifton RP, Mount DB. 2008. Roles of the cation - Chloride co-transporters in neurological disease. *Nat Clin Pract Neurol*. doi:10.1038/ncpneuro0883

Kaila K, Miles R. 2010. Chloride homeostasis and GABA signaling in temporal lobe epilepsy. *Epilepsia* **51**:52. doi:10.1111/j.1528-1167.2010.02838.x

Kaila K, Price TJ, Payne JA, Puskarjov M, Voipio J. 2014. Cation-chloride co-transporters in neuronal development, plasticity and disease. *Nat Rev Neurosci*. doi:10.1038/nrn3819

Kharod SC, Kang SK, Kadam SD. 2019. Off-label use of bumetanide for brain disorders: An overview. *Front Neurosci*. doi:10.3389/fnins.2019.00310

Kilkenny C, Browne WJ, Cuthill IC, Emerson M, Altman DG. 2010. Improving Bioscience Research Reporting: The ARRIVE Guidelines for Reporting Animal Research. *PLoS Biol* **8**:e1000412. doi:10.1371/journal.pbio.1000412

Lambertsen KL, Biber K, Finsen B. 2012. Inflammatory cytokines in experimental and human stroke. *J Cereb Blood Flow Metab*. doi:10.1038/jcbfm.2012.88

Lemonnier E, Degrez C, Phelep M, Tyzio R, Josse F, Grandgeorge M, Hadjikhani N, Ben-Ari Y. 2012. A randomised controlled trial of bumetanide in the treatment of autism in children. *Transl Psychiatry* **2**:202. doi:10.1038/tp.2012.124

Liu R, Wang J, Liang S, Zhang G, Yang X. 2020. Role of NKCC1 and KCC2 in Epilepsy: From Expression to Function. *Front Neurol*. doi:10.3389/fneur.2019.01407

Luheshi NM, Kovács KJ, Lopez-Castejon G, Brough D, Denes A. 2011. Interleukin-1α expression precedes IL-1β after ischemic brain injury and is localised to areas of focal neuronal loss and penumbral tissues. *J Neuroinflammation* **8**. doi:10.1186/1742-2094-8-186

Ma H, Li T, Tao Z, Hai L, Tong L, Yi L, Abeysekera IR, Liu P, Xie Y, Li J, Yuan F, Zhang C, Yang Y, Ming H, Yu S, Yang X. 2019. NKCC1 promotes EMT-like process in GBM via RhoA and Rac1 signaling pathways. *J Cell Physiol* **234**:1630–1642. doi:10.1002/jcp.27033

Madry C, Kyrargyri V, Arancibia-Cárcamo IL, Jolivet R, Kohsaka S, Bryan RM, Attwell D. 2018. Microglial Ramification, Surveillance, and Interleukin-1β Release Are Regulated by the Two-Pore Domain K + Channel THIK-1. *Neuron* **97**:299-312.e6. doi:10.1016/j.neuron.2017.12.002

Marguet SL, Le-Schulte VTQ, Merseburg A, Neu A, Eichler R, Jakovcevski I, Ivanov A, Hanganu-Opatz IL, Bernard C, Morellini F, Isbrandt D. 2015. Treatment during a vulnerable developmental period rescues a genetic epilepsy. *Nat Med* **21**:1436–1444. doi:10.1038/nm.3987

McColl BW, Rothwell NJ, Allan SM. 2007. Systemic inflammatory stimulus potentiates the acute phase and CXC chemokine responses to experimental stroke and exacerbates brain damage via interleukin-1- and neutrophil-dependent mechanisms. *J Neurosci* **27**:4403–4412. doi:10.1523/JNEUROSCI.5376-06.2007

Nguyen HM, Grössinger EM, Horiuchi M, Davis KW, Jin L-W, Maezawa I, Wulff H. 2017. Differential Kv1.3, KCa3.1, and Kir2.1 expression in "classically" and "alternatively" activated microglia. *Glia* **65**:106–121. doi:10.1002/glia.23078

Noor ZN, Deitmer JW, Theparambil SM. 2019. Cytosolic sodium regulation in mouse cortical astrocytes and its dependence on potassium and bicarbonate. *J Cell Physiol* **234**:89–99. doi:10.1002/jcp.26824

O'Donnell ME, Tran L, Lam TI, Liu XB, Anderson SE. 2004. Bumetanide inhibition of the blood-brain barrier Na-K-Cl co-transporter reduces edema formation in the rat middle cerebral artery occlusion model of stroke. *J Cereb Blood Flow Metab* **24**:1046–1056. doi:10.1097/01.WCB.0000130867.32663.90

Orsini F, Villa P, Parrella S, Zangari R, Zanier ER, Gesuete R, Stravalaci M, Fumagalli S, Ottria R, Reina JJ, Paladini A, Micotti E, Ribeiro-Viana R, Rojo J, Pavlov VI, Stahl GL, Bernardi A, Gobbi M, De Simoni MG. 2012. Targeting mannose-binding lectin confers long-lasting protection with a surprisingly wide therapeutic window in cerebral ischemia. *Circulation* **126**:1484–1494. doi:10.1161/CIRCULATIONAHA.112.103051

Otxoa-de-Amezaga A, Miró-Mur F, Pedragosa J, Gallizioli M, Justicia C, Gaja-Capdevila N, Ruíz-Jaen F, Salas-Perdomo A, Bosch A, Calvo M, Márquez-Kisinousky L, Denes A, Gunzer M, Planas AM. 2019. Microglial cell loss after ischemic stroke favors brain neutrophil accumulation. *Acta Neuropathol* **137**:321–341. doi:10.1007/s00401-018-1954-4

Percie du Sert N, Alfieri A, Allan SM, Carswell HVO, Deuchar GA, Farr TD, Flecknell P, Gallagher L, Gibson CL, Haley MJ, Macleod MR, McColl BW, McCabe C, Morancho A, Moon LDF, O'Neill MJ, Pérez de Puig I, Planas A, Ragan CI, Rosell A, Roy LA, Ryder KO, Simats A, Sena ES, Sutherland BA, Tricklebank MD, Trueman RC, Whitfield L, Wong R, Macrae IM. 2017. The IMPROVE Guidelines (Ischaemia Models: Procedural Refinements Of in Vivo Experiments). *J Cereb Blood Flow Metab*. doi:10.1177/0271678X17709185

Pozdeev VI, Lang E, Görg B, Bidmon HJ, Shinde P V., Kircheis G, Herebian D, Pfeffer K, Lang F, Häussinger D, Lang KS, Lang PA. 2017. TNFα induced up-regulation of Na+,K+,2Cl− co-transporter NKCC1 in hepatic ammonia clearance and cerebral ammonia toxicity. *Sci Rep* **7**. doi:10.1038/s41598-017-07640-8

Pressler RM, Boylan GB, Marlow N, Blennow M, Chiron C, Cross JH, de Vries LS, Hallberg B,

Hellström-Westas L, Jullien V, Livingstone V, Mangum B, Murphy B, Murray D, Pons G, Rennie J, Swarte R, Toet MC, Vanhatalo S, Zohar S. 2015. Bumetanide for the treatment of seizures in newborn babies with hypoxic ischaemic encephalopathy (NEMO): an open-label, dose finding, and feasibility phase 1/2 trial. *Lancet Neurol* **14**:469–477. doi:10.1016/S1474-4422(14)70303-5

Puskarjov M, Kahle KT, Ruusuvuori E, Kaila K. 2014. Pharmacotherapeutic targeting of cation-chloride co-transporters in neonatal seizures. *Epilepsia*. doi:10.1111/epi.12620

Rahmanzadeh R, Shahbazi A, Ardakani M reza K, Mehrabi S, Rahmanzade R, Joghataei MT. 2017. Lack of the effect of bumetanide, a selective NKCC1 inhibitor, in patients with schizophrenia: A double-blind randomized trial. *Psychiatry Clin Neurosci*. doi:10.1111/pcn.12475

Reid AY, Riazi K, Campbell Teskey G, Pittman QJ. 2013. Increased excitability and molecular changes in adult rats after a febrile seizure. *Epilepsia* **54**. doi:10.1111/epi.12061

Rivera C, Voipio J, Payne JA, Ruusuvuori E, Lahtinen H, Lamsa K, Pirvola U, Saarma M, Kaila K. 1999. The K+/Cl- co-transporter KCC2 renders GABA hyperpolarizing during neuronal maturation. *Nature* **397**:251–255. doi:10.1038/16697

Römermann K, Fedrowitz M, Hampel P, Kaczmarek E, Töllner K, Erker T, Sweet DH, Löscher W. 2017. Multiple blood-brain barrier transport mechanisms limit bumetanide accumulation, and therapeutic potential, in the mammalian brain. *Neuropharmacology* **117**:182–194. doi:10.1016/j.neuropharm.2017.02.006

Russell JM. 2000. Sodium-potassium-chloride cotransport. *Physiol Rev*. doi:10.1152/physrev.2000.80.1.211

Salter MW, Stevens B. 2017. Microglia emerge as central players in brain disease. *Nat Med 2017 239* **23**:1018–1027. doi:10.1038/nm.4397

Schaar KL, Brenneman MM, Savitz SI. 2010. Functional assessments in the rodent stroke model. *Exp Transl Stroke Med*. doi:10.1186/2040-7378-2-13

Schiapparelli P, Guerrero-Cazares H, Magaña-Maldonado R, Hamilla SM, Ganaha S, Goulin Lippi Fernandes E, Huang CH, Aranda-Espinoza H, Devreotes P, Quinones-Hinojosa A. 2017. NKCC1 Regulates Migration Ability of Glioblastoma Cells by Modulation of Actin Dynamics and Interacting with Cofilin. *EBioMedicine* **21**:94–103. doi:10.1016/j.ebiom.2017.06.020

Schulte JT, Wierenga CJ, Bruining H. 2018. Chloride transporters and GABA polarity in developmental, neurological and psychiatric conditions. *Neurosci Biobehav Rev*. doi:10.1016/j.neubiorev.2018.05.001

Shekarabi M, Zhang J, Khanna AR, Ellison DH, Delpire E, Kahle KT. 2017. WNK Kinase Signaling in Ion Homeostasis and Human Disease. *Cell Metab*. doi:10.1016/j.cmet.2017.01.007

Song WM, Colonna M. 2018. The identity and function of microglia in neurodegeneration. *Nat Immunol*. doi:10.1038/s41590-018-0212-1

Steffensen AB, Oernbo EK, Stoica A, Gerkau NJ, Barbuskaite D, Tritsaris K, Rose CR, MacAulay N. 2018. Cotransporter-mediated water transport underlying cerebrospinal fluid

formation. *Nat Commun* **9**. doi:10.1038/s41467-018-04677-9

Su G, Kintner DB, Flagella M, Shull GE, Sun D. 2002. Astrocytes from Na(+)-K(+)-Cl(-) cotransporter-null mice exhibit absence of swelling and decrease in EAA release. *Am J Physiol Cell Physiol* **282**:C1147-60. doi:10.1152/ajpcell.00538.2001

Swanson K V., Deng M, Ting JPY. 2019. The NLRP3 inflammasome: molecular activation and regulation to therapeutics. *Nat Rev Immunol*. doi:10.1038/s41577-019-0165-0

Swertz MA, Dijkstra M, Adamusiak T, van der Velde JK, Kanterakis A, Roos ET, Lops J, Thorisson GA, Arends D, Byelas G, Muilu J, Brookes AJ, De Brock EO, Jansen RC, Parkinson H. 2010. The MOLGENIS toolkit: Rapid prototyping of biosoftware at the push of a button. *BMC Bioinformatics* **11**. doi:10.1186/1471-2105-11-S12-S12

Szalay G, Martinecz B, Lénárt N, Környei Z, Orsolits B, Judák L, Császár E, Fekete R, West BL, Katona G, Rózsa B, Dénes Á. 2016. Microglia protect against brain injury and their selective elimination dysregulates neuronal network activity after stroke. *Nat Commun* **7**:11499. doi:10.1038/ncomms11499

Töllner K, Brandt C, Römermann K, Löscher W. 2015. The organic anion transport inhibitor probenecid increases brain concentrations of the NKCC1 inhibitor bumetanide. *Eur J Pharmacol* **746**:167–173. doi:10.1016/j.ejphar.2014.11.019

Virtanen MA, Uvarov P, Hübner CA, Kaila K. 2020. NKCC1, an Elusive Molecular Target in Brain Development: Making Sense of the Existing Data. *Cells* **9**:2607. doi:10.3390/cells9122607

Wang H, Yan Y, Kintner DB, Lytle C, Sun D. 2003. GABA-mediated trophic effect on oligodendrocytes requires Na-K-2Cl cotransport activity. *J Neurophysiol* **90**:1257–1265. doi:10.1152/jn.01174.2002

Watanabe M, Fukuda A. 2015. Development and regulation of chloride homeostasis in the central nervous system. *Front Cell Neurosci* **9**:371. doi:10.3389/fncel.2015.00371

Weidenfeld S, Kuebler WM. 2017. Cytokine-regulation of Na+-K+-Cl- cotransporter 1 and cystic fibrosis transmembrane conductance regulator-potential role in pulmonary inflammation and edema formation. *Front Immunol*. doi:10.3389/fimmu.2017.00393

Wendeln AC, Degenhardt K, Kaurani L, Gertig M, Ulas T, Jain G, Wagner J, Häsler LM, Wild K, Skodras A, Blank T, Staszewski O, Datta M, Centeno TP, Capece V, Islam MR, Kerimoglu C, Staufenbiel M, Schultze JL, Beyer M, Prinz M, Jucker M, Fischer A, Neher JJ. 2018. Innate immune memory in the brain shapes neurological disease hallmarks. *Nature* **556**:332–338. doi:10.1038/s41586-018-0023-4

Wofford KL, Loane DJ, Cullen DK. 2019. Acute drivers of neuroinflammation in traumatic brain injury. *Neural Regen Res*. doi:10.4103/1673-5374.255958

Wu D, Zhang G, Zhao C, Yang Y, Miao Z, Xu X. 2020. Interleukin-18 from neurons and microglia mediates depressive behaviors in mice with post-stroke depression. *Brain Behav Immun* **88**:411–420. doi:10.1016/j.bbi.2020.04.004

Yamada J, Okabe A, Toyoda H, Kilb W, Luhmann HJ, Fukuda A. 2004. Cl- uptake promoting depolarizing GABA actions in immature rat neocortical neurones is mediated by NKCC1. *J Physiol* **557**:829–841. doi:10.1113/jphysiol.2004.062471

Yona S, Kim K-W, Wolf Y, Mildner A, Varol D, Breker M, Strauss-Ayali D, Viukov S, Guilliams M, Misharin A, Hume DA, Perlman H, Malissen B, Zelzer E, Jung S. 2013. Fate Mapping Reveals Origins and Dynamics of Monocytes and Tissue Macrophages under Homeostasis. *Immunity* **38**:79–91. doi:10.1016/j.immuni.2012.12.001

Yu Y, Fu P, Yu Z, Xie M, Wang W, Luo X. 2018. NKCC1 Inhibition Attenuates Chronic Cerebral Hypoperfusion-Induced White Matter Lesions by Enhancing Progenitor Cells of Oligodendrocyte Proliferation. *J Mol Neurosci* **64**:449–458. doi:10.1007/s12031-018-1043-0

Zhang Jinwei, Bhuiyan MIH, Zhang T, Karimy JK, Wu Z, Fiesler VM, Zhang Jingfang, Huang H, Hasan MN, Skrzypiec AE, Mucha M, Duran D, Huang W, Pawlak R, Foley LM, Hitchens TK, Minnigh MB, Poloyac SM, Alper SL, Molyneaux BJ, Trevelyan AJ, Kahle KT, Sun D, Deng X. 2020. Modulation of brain cation-Cl− cotransport via the SPAK kinase inhibitor ZT-1a. *Nat Commun* **11**:Zhang, J., Bhuiyan, M. I. H., Zhang, T., Karimy, J. doi:10.1038/s41467-019-13851-6

Zhang Y, Chen K, Sloan SA, Bennett ML, Scholze AR, O'Keeffe S, Phatnani HP, Guarnieri P, Caneda C, Ruderisch N, Deng S, Liddelow SA, Zhang C, Daneman R, Maniatis T, Barres BA, Wu JQ. 2014. An RNA-sequencing transcriptome and splicing database of glia, neurons, and vascular cells of the cerebral cortex. *J Neurosci* **34**:11929–11947. doi:10.1523/JNEUROSCI.1860-14.2014

Supplemental Material

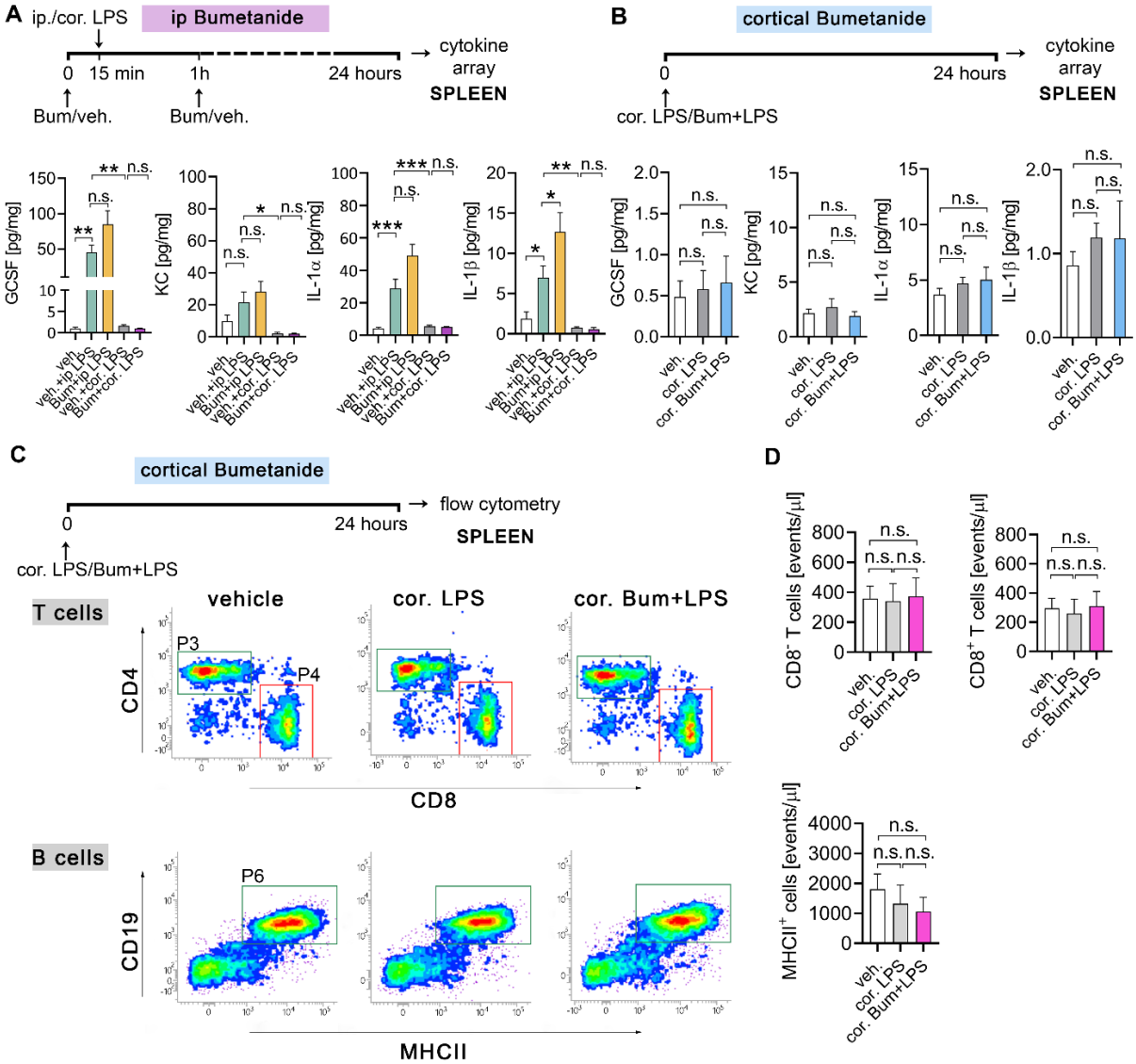

Supplementary Figure 1. Effects of systemic vs. central blockade of NKCC1 on LPS-induced cytokine responses in the periphery. A: Intraperitoneal bumetanide (Bum) injections further enhance the ip. LPS-induced GCSF, IL-1α and IL-1β production, while intracortical LPS alone or with Bum has no significant effect on cytokine levels in the spleen. **B:** Intracortical (cor.) LPS injection does not induce cytokine production in the spleen and Bum has no effect on baseline cytokine levels in the spleen. Similar results were obtained from liver samples (data not shown). **C-D:** Flow cytometric dot plots show that cortical administration of Bum does not alter the numbers of $CD4^+$ (P3 gate) and $CD8^+$ (P4 gate) T cells and $CD19^+$ $MHCII^+$ (P6 gate) B cells in the spleen. All data are expressed as mean±SEM. **A**: One-way ANOVA followed by Tukey's multiple comparison test; *p<0.05; **p<0.01; ***p<0.001; N=6/group; **B:** Unpaired t-test; *p<0.05; N=9/group. **D:** One-way ANOVA followed by Tukey's multiple comparison test; N=4/group Abbreviations: veh.: vehicle; ip: intraperitoneal; cor.: cortical; Bum: bumetanide; n. s.: not significant

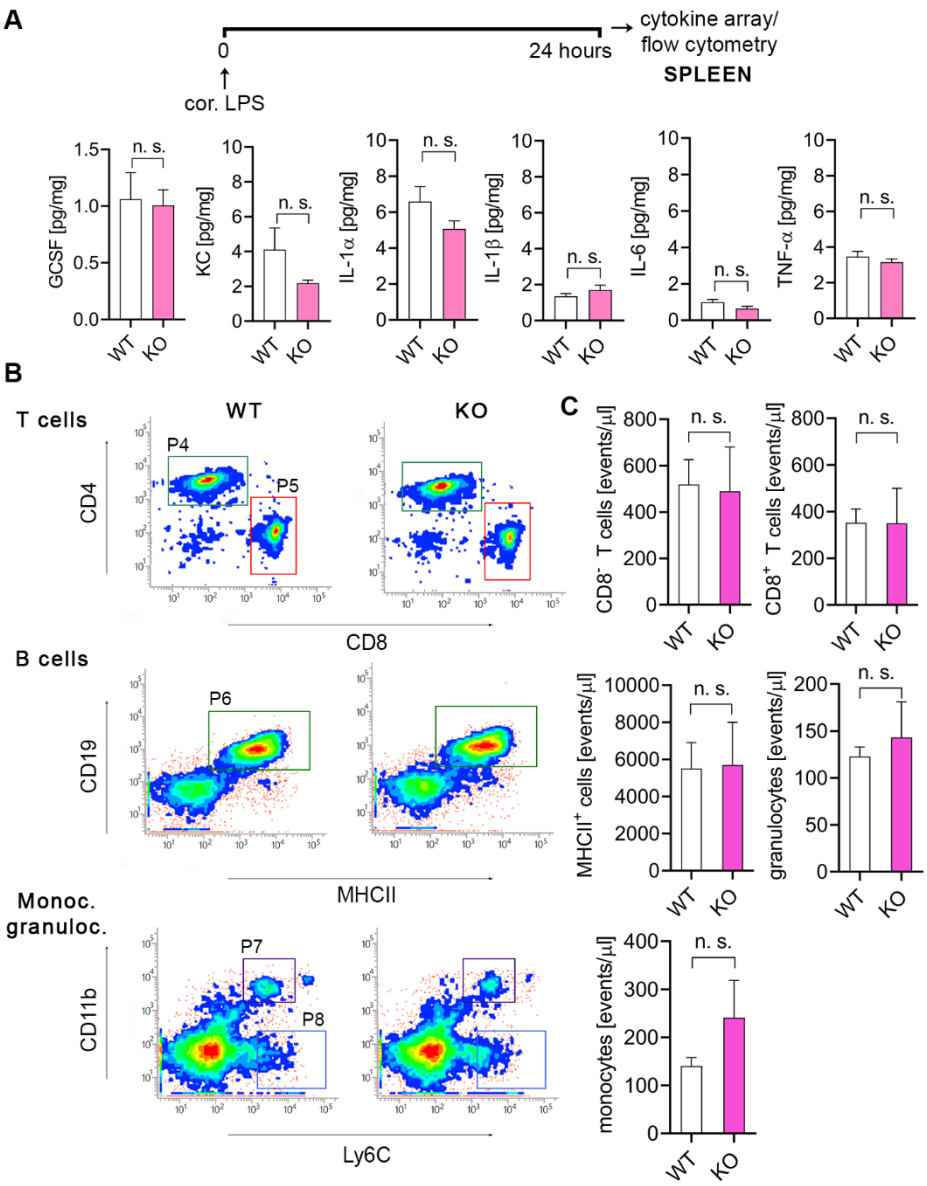

Supplementary Figure 2. Microglial NKCC1 deficiency does not alter cytokine levels and main leukocyte populations in the spleen after intracortical LPS injection. A: Cytokine levels in the spleen do not differ between WT and NKCC1 KO mice after intracortical LPS administration. **B-C:** Numbers of $CD4^+$ (P4 gate), $CD8^+$ (P5 gate) T cells, and $CD19^+$ $MHCII^+$ B cells (P6 gate) are not altered in the spleen of NKCC1 KO mice compared to WT. Microglial NKCC1 deficiency does not affect the proportion of monocytes (P8 gate) or granulocytes (P7 gate) compared to WT. **A:** Mann-Whitney test, *: p <0.05; N (WT)=7, N (KO) =6; **C:** Unpaired t-test; N (WT)=4, N (KO)=4; n. s.: not significant